COVER LETTER

bg-2014-318

Dear Dr. Micol Rossini,

first of all, we would like to thank you and the reviewers for recognizing our efforts made to improve upon the previous version of the manuscript.

With this writing we submit a revised version of our paper for publication in BG. The paper was revised according to the reviewer comments. In particular, we included additional statistical metrics to the validation in order to demonstrate the applicability of our methodology and the robustness of our findings.

In summary, we were thus able to address all reviewer comments in the revised manuscript and hope that the manuscript is now acceptable for publication in BG.

All main changes relative to the previous version of the manuscript are detailed in the pdf of the new manuscript in blue. All technical and grammar corrections are included in the revised version of the manuscript.

The authors' response to the comments of reviewer is enclosed.

Main changes:

Text

Abstract: this part was revised according to the suggestion of the reviewer.

Section 3.4 "Evaluation of the model performance": this section was completely rewritten by including the new error metrics.

Tables

Table 1 revised by eliminating the details on the eddy covariance systems and data acquisition and processing. The caption was corrected accordingly.

Table 5 revised by substituting r with R^2 and eliminating the band centers. The caption was corrected accordingly.

New Table S1 in the supplemental section with the details on the eddy covariance systems and data acquisition and processing was added (data from previous version of Table 1). The caption was modified accordingly.

Table S1 in the supplemental section **was renumbered** as Table S3.

New Table S4 in the supplemental section with the error metrics of the validation at midday scale was added.

New Table S5 in the supplemental section with the error metrics of the validation at daily scale was added.

Table S3 in the supplemental section **was renumbered** as Table S6.

Figures

Figure 1 was revised by replacing the asterisk with a white dot. The caption was corrected accordingly**.**

Figure 3 was moved from the main text to the supplemental section and renamed as Figure S1.

Old figures 4-6 (now Figs. 3-5) **were revised** by using R^2 superscripted. The asterisks were replaced by white dots and the size was increased. The caption was corrected accordingly.

Figures 4-11 were renumbered as Figs. 3-10.

Old figure 8 (now Fig. 7) **was revised** by replacing r with R^2. The caption was modified accordingly.

Figures S1-S10 in the supplemental section **were renumbered** as Figs. S2-S11**.**

Old figure S9 in the Supplemental material (now S10) **was revised** by replacing r with R^2. The caption was modified accordingly.

References

The following references were eliminated from the main text

Jacquemoud, S., and Baret, F.: PROSPECT: a model of leaf optical properties spectra, Remote Sens. Environ., 34, 75–91, 1990.

Verhoef, W.: Light scattering by leaves with application to canopy reflectance modelling: the SAIL model, Remote Sens. Environ., 16, 125–178, 1984.

Comment on "On the relationship between ecosystem-scale hyperspectral reflectance and CO_2 exchange in European mountain grasslands" by M. Balzarolo et al.

Anonymous Referee #2
Report on: report 13 Mar 2015

Specific Comments:
Fortunately, the authors have thoughtfully responded to my earlier criticisms and addressed many of them to the best of their ability considering the limitations of the methods utilized in the implementation of their study. Because of this effort, the manuscript has been greatly improved. However, there are still several major issues that need to be addressed before it is suitable for publication. I have grave concern regarding the validation procedure. There was strong correlations between measured and simulated results; however, these did not follow the expected 1:1 line. The manuscript still has a large number of figures and tables which probably could be summarized or excluded from the manuscript as they do not provide a major support to the findings. Language is also a major problem with many run-on sentences and awkward phrases.

The authors acknowledge the unknown reviewer for recognizing their efforts made to improve upon the previous version of the manuscript. We have taken the reviewer comments into account and revised the manuscript accordingly. In particular we have added error metrics to strengthen the validation of the linear models. Thanks also for the helpful suggestions to improve clarity and readability of the manuscript. Please see the following responses to the specific comments.

Specific Comments:

P16L23: Correlation is not informative as an error metric for validation. There are several relationships in Figure 8 that have relatively high r values but clearly do not have a linear 1:1 relationship between measured and simulated values. The error metrics need to be determined from the 1:1 line, which will demonstrate that ε was not transferable at all. It is a stretch to say that some of the other models were also transferable. Likely there is some measure of bias which should also be reported to readers.

We agree with this comment and added the error metrics for the linear models to the revised manuscript. In particular, we now show the following statistical metrics: slope and y-intercept of the linear model and root mean square error (RMSE). Based on these additional statistics we

have re-written section 3.4 on the evaluation of model performance and the corresponding section in the discussion. The new tables S4 and S5 containing the statistical metrics of the validations were added to the Supplemental material. Figure 8 (now Fig. 7) and figure S9 in the Supplemental material (now Fig. S10) were revised by replacing r with R^2.

Table 1: Is all of this information necessary? Focus on the key points necessary for readers to understand how the study was conducted.

We added some information to the Table 1 (e.g. eddy system description) in answering to the comments of the other reviewer during the first revision iteration. However, Table 1 was again revised by removing the details on the eddy covariance data acquisition and processing. These details are described in the section "2.4 CO_2 flux measurements" and reported in the new Table S1 in the supplemental section.

Table 5: Why use r instead of R^2? Generally it would be good to report the band centers; however, this table is already pretty complex and these values were already reported on the Figures. They could probably be dropped here to improve the readability.

As requested, we replaced r with R^2. Table 5 revised by removing the columns with the bands centers. Also the old Table S3, now renumbered as Table S4, in the Supplemental material was revised accordingly.

Figure 3: Is this figure really necessary?

We agree. The Figure 3 is not really necessary, although it gives the reader an impression of some of the raw data underlying the analysis; therefore it was moved from the main text to the Supplemental material and renamed as Fig. S1. The corresponding former text was reduced down to a single line.

Figure 4-6: The R^2 should be superscripted on the figures themselves after the x and y values. The asterisks are very difficult to see. Please increase their size.

Thanks, we corrected the text of these figures and the corresponding figures in the Supplemental material.

Figure 8: r values clearly do not demonstrate transferability for several of these validated parameters.

We agree with this comment and we added to the revised manuscript the error metrics for the found linear models as reported by answering to the specific comment P16L23 (see above).

Technical Corrections:

P2L1: Rephrase “VIs derived from hyperspectral data”

Done

P2L3: Results usually doesn’t ‘exhibit skill’. Also, more than what? What were the VIs compared to? Specifically address that this study also examined traditional VIs.

The abstract was re-written accordingly.

P1L19-P2L14: There are several run-on sentences in the abstract. I suggest shortening them into smaller sentences. This seems to be common elsewhere in the manuscript as well.

The abstract was revised and rewritten in the revised version of the manuscript.

P2L28-P3L2: Open-ended parentheses.

Thanks, we corrected it.

P3L7: Another open-ended parentheses. This seems to be common whenever there was an ‘e.g.’

Thanks, we corrected it.

P3L8-19: There is too much discussion on PROSAIL and it isn’t used in the manuscript. It is an alternative method. Be more concise and focus on the relevant previously published results using this method.

This part was rewritten in the revised version of the manuscript and any explicit mentioning of PROSAIL removed.

P5L4-8: This is awkwardly written.

This sentence was re-worded in the revised version of the manuscript.

P5L10: Break this into two sentences.

We agree and we divided into two parts these sentence.

P5L24-28: Run-on sentence.

This sentence was re-worded.

P5L28-P6L3: Run-on sentence.

This sentence was re-worded.

P8L4-6: Serial numbers are not necessary.

We added the serial numbers of the instruments since this was asked for by the other reviewer. However, we agree that the serial numbers are not relevant. Therefore, to make this part more readable we eliminated the serial numbers from the text in the revision version of the manuscript.

P13L15: Use past tense ‘was evident’.

Thanks, we corrected it.

P13L15-19: Run-on sentence.

Sentence was re-worded.

P13L20-23: Run-on sentence.

Sentence was re-worded.

P14L24-27: Run-on sentence.

Sentence was re-worded.

On the relationship between ecosystem-scale hyperspectral reflectance and CO_2 exchange in European mountain grasslands

M. Balzarolo[1], L. Vescovo[2,3], A. Hammerle[4], D. Gianelle[2,3], D. Papale[5], E. Tomelleri[6], G. Wohlfahrt[4,6]

[1]{PLECO research group, University of Antwerpen, Wilrjik, Belgium}

[2]{Forests and Biogeochemical Cycles Research Group, Sustainable Agro-Ecosystems and Bioresources Department, Research and Innovation Centre – Fondazione Edmund Mach, S. Michele all'Adige (TN), Italy}

[3]{FoxLaB Research and Innovation Centre - Fondazione Edmund Mach, S. Michele all'Adige (TN), Italy}

[4]{Institute of Ecology, University of Innsbruck, Innsbruck, Austria}

[5]{DIBAF, University of Tuscia, Viterbo, Italy}

[6]{European Academy of Bolzano, Bolzano, Italy}

Correspondence to: M. Balzarolo (manuela.balzarolo@uantwerpen.be)

Abstract

In this paper we explore the skill of hyperspectral reflectance measurements and vegetation indices (VIs) derived therefrom in estimating carbon dioxide (CO_2) fluxes ~~(net ecosystem exchange – NEE; gross primary production – GPP), and some key ecophysiological variables related to NEE and GPP (light use efficiency – ε; initial quantum yield – α; and GPP at saturating light – GPP_{max})~~ of grasslands. Hyperspectral reflectance data ~~(400-1000 nm)~~, CO_2 fluxes and biophysical parameters were measured at three grassland sites located in European mountain regions using standardized protocols. The relationships between CO_2 fluxes, ecophysiological variables, traditional VIs and VIs derived using all two-band combinations of

wavelengths available from the whole hyperspectral data space were analysed. We found that ~~hyperspectral VIs~~ VIs derived from hyperspectral data generally explained a large fraction of the variability in the investigated dependent variables, but differed in their ability to estimate midday and daily average CO_2 fluxes and various derived ecophysiological parameters ~~and that they generally exhibited more skill in estimating midday and daily average GPP and NEE, as well as GPP_{max}, than α and ε~~. Relationships between VIs and CO_2 fluxes and ecophysiological parameters were site-specific, likely due to differences in soils, vegetation parameters and environmental conditions. Chlorophyll and water content related VIs ~~(e.g. CI, NPCI, WI), reflecting seasonal changes in biophysical parameters controlling the photosynthetic process,~~ explained the largest fraction of variability in most of the dependent variables. Band selection based on a combination of a genetic algorithm with random forests (GA-rF) confirmed that it is difficult to select a universal band region suitable ~~for describing ecophysiological parameters, CO_2 fluxes and biophysical variables~~ across the investigated ecosystems. Our findings have major implications for up-scaling terrestrial CO_2 fluxes to larger regions and for remote and proximal sensing sampling and analysis strategies and call for more cross-site synthesis studies linking ground-based spectral reflectance with ecosystem-scale CO_2 fluxes.

1 Introduction

Understanding the mechanisms that drive the carbon dioxide (CO_2) exchange of terrestrial ecosystems is one of the main challenges for ecologists working on climate change (Beer et al., 2010). Plant gross photosynthesis, also referred to as gross primary productivity (GPP), is one of the major components of the global carbon cycle. It interacts in complex ways with environmental factors such as radiation, nutrients, soil moisture, vapor pressure deficit, air temperature and soil temperature (Drolet et al. 2005). Plant biochemistry and structure determine many fundamental ecosystem patterns, processes and dynamics (Lambers et al. 1998; Waring and Running 1998). The canopy nitrogen content regulates the canopy photosynthetic capacity and the canopy light use efficency (ε) (Ollinger et al., 2008). In addition, the canopy chlorophyll content plays an important role in controlling ecosystem photosynthesis and carbon gain (Peng et al., 2011; Gitelson et al., 2006).

Optical remote sensing can help ecologists in qualitatively and quantitatively assessing plant and canopy properties (e.g. biomass (Vescovo et al. 2012), water content (Clevers et al., 2010), nitrogen content (Ollinger et al., 2008; Knyazikhin et al., 2012), chlorophylls (Gitelson et al., 2006) and photosynthetic rate (Inoue et al., 2008) that drive ecosystem processes related to the carbon cycle).

Empirical and physical based methods have been proposed by several authors to interpret optical plant and canopy properties. Empirical methods consist of, for example, linear regression analysis between plant or canopy properties and optical data. The most used empirical methods are: hyperspectral index methods (Peñuelas et al., 1993; Sims and Gamon, 2002; Inoue et al., 2008) and multi-variable statistical methods, (e.g. stepwise linear regression, genetic algorithm, neural network (Grossman et al., 1996; Riaño et al., 2005a; Li et al., 2007). Physical methods are based on the use of radiative transfer models (RTMs) to simulate light absorption and scattering through the canopy as a function of canopy structure and leaf biochemical composition (Jacquemoud et al., 2000; Zarco-Tejada et al., 2003). Therefore, RTMs help in quantifying the contribution of canopy biophysical and biochemical variables to canopy reflectance. ~~One of the most popular RTM is PROSAIL, based on the coupling of the SAIL canopy bidirectional reflectance model (Verhoef et al., 1984) and the PROSPECT leaf optical properties model (Jacquemoud and Baret, 1990).~~ Such models can be used for identifying regions of the light spectrum that are of particular importance for specific biophysical properties of vegetation. ~~The sensitivity analysis of the PROSAIL model~~ For example, it was demonstrated that the red-edge region (between 680 nm to 730 nm) of the spectrum is sensitive to the leaf chlorophyll content and leaf area index (LAI) (Baret et al., 1992). It is also well accepted that an increase of LAI includes a decrease of reflectance in the red and an increase in the near-infrared (NIR) region (Jacquemoud, 1993). In the NIR region, effects of LAI and the leaf angle distribution equally contribute to the reflectance response (Bacour et al., 2002a). NIR reflectance between 800 nm and 850 nm is also related to canopy N content (Ollinger et al., 2008; Knyazikhin et al., 2012). In addition, the combination of the reflectance in NIR and in the short wave infrared region (SWIR) is correlated with canopy water content (Colombo et al., 2008), but the reflectance between 1000 nm and 1400 nm is also highly sensitive to LAI. So, some attention is needed when these spectral regions are used to retrieve water content considering that the canopy properties in a given ecosystem often co-vary (Bacour et al., 2002b).

The drawback of such an approach consists in the fact that the process of building a model implies approximations and assumptions. For this reason we opted for a purely data based approach such as the hyperspectral index approach. This method consists of the use of spectral vegetation indices (VIs) defined as spectral band ratios, or normalized band ratios between the reflectance in the visible (VIS) vs. NIR region or VIS vs. VIS or NIR vs. NIR.

The typical optical sampling approach, which is linking spectral observations with CO_2 fluxes, is based on the Monteith equation (1972, 1977):

$$GPP = \varepsilon * PAR * fAPAR \quad (1)$$

where ε is the light use efficiency and fAPAR is the fraction of absorbed photosynthetically active radiation); both ε and fAPAR can be retrieved by remote optical observations. A wide number of VIs that can potentially be used to model the productivity of terrestrial ecosystems (as a proxy of ε and fAPAR) has been suggested (Inoue et al., 2008; Coops et al., 2010; Peñuelas et al., 2011; Rossini et al. 2012). The various VIs differ in their sensitivity to changes in photosynthetic status. "Greeness indices" – such the widely used Normalized Difference Vegetation Index (NDVI) – demonstrated to be a good proxy for fAPAR, but are not sensitive to rapid changes in plant photosynthesis which are induced by common environmental and anthropogenic stressors (Gitelson et al., 2008; Hmimina et al., 2014; Soudani et al., 2014). However, in ecosystems characterized by strong dynamics (e.g. grasslands and crops with a strong green-up and senescence), other VIs are able to effectively monitor seasonal changes in biophysical parameters controlling canopy photosynthesis such as fAPAR and chlorophyll content and consequently, can be adopted to monitor the seasonal and spatial variability of carbon fluxes (Gitelson et al., 2012; Sakowska et al., 2014). Short-term changes in ε can be remotely detected through a spectral proxy of the xanthophyll cycle (Photochemical Reflectance Index, PRI; Gamon et al., 1992). The PRI is one of the most promising VIs for a direct estimation of photosynthetic light use efficiency and of its seasonal and diurnal variations (Nichol et al., 2002). Latest developments of the sun-induced fluorescence method may allow even more direct remote sensing of plant photosynthesis in the near future (Meroni et al., 2009; Rossini et al., 2010; Frankenberg et al., 2011). At canopy scale, the relationship between PRI and ε was shown to be site-dependent (Garbulsky et al., 2011; Goerner et al., 2011) and strongly affected by environmental conditions (Soudani et al. 2014).

Whereas previous studies have demonstrated the ability of remote sensing data to allow modelling ecosystem GPP at ecosystem scale (e.g. Gianelle et al., 2009; Wohlfahrt et al., 2010; Rossini et al. 2012; Sakowska et al., 2014), a universal model for GPP estimation applicable across different ecosystems and a wide range of environmental conditions is still missing. ~~In addition, p~~Previous studies often focussed on single sites with specific characteristics (e.g. climate, vegetation composition, soil type; see Wohlfahrt et al., 2010). ~~and~~ In addition, different studies ~~were~~ often ~~based on the use of~~ used different sensors, platforms and protocols (Balzarolo et al., 2011), making generalisation difficult. Moreover, most of the studies have either relied on reflectance measurements in a few spectral wavebands (e.g. Wohlfahrt et al., 2010 and Sakowska et al, 2014) ~~or a minimum number of bands needed to calculate the most common VIs~~, missing potentially important information in under-sampled spectral regions ~~that could help explain carbon fluxes and variability~~. In order to overcome such heterogeneity in spectrometry measurements, SpecNet (http://specnet.info; Gamon et al., 2006), the European COST Action ES0903 (EUROSPEC; http://cost-es0903.fem-environment.eu/) and the COST Action ES1309 (OPTIMISE; http://www.cost.eu/domains_actions/essem/Actions/ES1309) focused on the definition of a standardized protocol for making optical measurements at the eddy covariance CO_2 flux towers (Gamon et al., 2010).

The overarching objective of the present paper is thus to develop a common framework for predicting grassland carbon fluxes and ecophysiological parameters based on optical remote sensing data across measurement sites exposed to diverse natural (climate) and anthropogenic (management) factors. To this end we combine eddy covariance CO_2 flux measurements with ground-based hyperspectral reflectance measurements for six different grasslands in Europe. In order to make the optical and fluxes measurements comparable, these were acquired at the six sites following a common protocol resulting in a unique standardized data set. We focused on European grasslands, which ~~since~~ cover~~ing~~ roughly 22% (80 million ha) of the EU-25 land area~~, grasslands~~ and are thus among the dominating ecosystem types in Europe (EEA, 2005). Accordingly ~~and~~ their role in the European carbon balance has received a lot of scientific interest (Soussana et al., 2007; Gilmanov et al., 2007; Wohlfahrt et al., 2008; Ciais et al. 2010). ~~While d~~Direct measurements of the grassland carbon exchange have been carried out and are still ongoing at a number of different grassland sites in Europe ~~notably in the two EU projects GreenGrass~~ (e.g. Soussana et al., 2007; ~~) and CarboMont (~~Cernusca et al., 2008). ~~s~~Scaling up

these plot-level measurements to the continental scale requires a modelling approach, typically based on or supported by remotely sensed data. Therefore, we believe that this study will improve the current knowledge on modelling the carbon dynamics of European grasslands.

2 Materials and methods

2.1 Experimental site description

This study was carried out at six experimental mountain grassland sites in Europe covering different climatic and grassland management conditions existing in the mountain regions of Europe, which were already part of the preceding study by Vescovo et al. (2012). This dataset combined *in-situ* hyperspectral, biophysical and flux measurements based on common protocol (for more details see sect. 2.2, sect. 2.3 and sect. 2.4). This dataset is unique since no common protocol for hyperspectral measurements exists in the various eddy covariance networks (e.g. FLUXNET). In this study, three of these sites (Amplero, Neustift and Monte Bondone, see Table 1 and S1 in the Supplemental section) composed the main dataset used in the analysis, while the other three sites (Table S2 in Supplemental section) were used to independently validate the models obtained with the main dataset.

Main study sites (Table 1 and S1 in the Supplemental section):

Amplero

The Amplero site is situated in the Mediterranean Appennine mountain region of Italy (41.90409 N, 13.60516 E) at 884 m a.s.l.. This site is characterized by mild, rainy winters and by an intense drought in summer. Amplero is managed as a hay meadow with one cut in late June and extensive grazing during summer and autumn.

Monte Bondone

The Monte Bondone site is situated in the Italian Alps (46.01468 N, 11.04583 E) at 1550 m a.s.l.. This site is characterized by a typical sub-continental climate with mild summers and

precipitation peaks in spring and autumn. Monte Bondone is managed as an extensive meadow with one cut in mid-July.

Neustift

The Neustift grassland site is located in the Austrian Alps (47.11620 N, 11.32034 E) at 970 m a.s.l.. The climate of this area is continental/Alpine, with precipitation peaks during the summer (July). This site is intensively managed as a hay meadow with three cuts in mid-June, beginning of August and at the end of September.

Validation sites:

Längenfeld

The site Längenfeld is located in the Austrian Alps (47.0612 N, 10.9634 E) at 1180 m a.s.l.. The climate of this area is continental/Alpine, however compared to the other Alpine sites in this study, the site receives comparably less precipitation due to rain shadowing effects from both the North and South. The site is intensively managed as a hay meadow with three cuts in mid-June, mid-August and mid-October.

Leutasch

The site Leutasch is located in the Austrian Alps (47.3780 N, 11.1627 E) at 1115 m a.s.l.. The climate of this area is Alpine with substantial precipitation due to its position on the north range of the Alps. The site is extensively managed as a hay meadow with two cuts at the end of June and beginning of September.

Scharnitz

The site Scharnitz is located very close to Leutasch (47.3873 N, 11.2479 E) at 964 m a.s.l. and the climate is thus very similar to Leutasch. The site is extensively managed as a hay meadow with two cuts at the beginning of July and beginning of September.

2.2 Hyperspectral reflectance measurements

The canopy hyperspectral reflectance measurements were collected at each site under clear sky conditions close to solar noon (between 11:00 to 14:00 Central European time) using the same model of a portable spectroradiometer (ASD FieldSpec HandHeld, Inc., Boulder, CO, USA~~; serial numbers: 1275 for Amplero, 6354 for Monte Bondone in 2006/2013 and 1191 for Neustift, Längenfeld, Leutasch, Scharnitz and Monte Bondone in 2005~~) at all sites. The spectroradiometer acquires reflectance values between 350 and 1075 nm with a Full Width Half Maximum (FWHM) of 3.5 nm and a spectral resolution of 1 nm. In order to achieve a better match between the eddy covariance flux footprint and optical measurements, a cosine diffuser foreoptic (ASD Remote Cosine Receptor, Inc., Boulder, CO, USA), calibrated by the manufacture, was used for nadir/zenith measurements (Gianelle et al., 2009; Fava et al., 2009; Meroni et al. 2011). The ASD's cosine receptor is designed with a geometry and material that provides a hemispherical field of view (FOV) of 180˚ and optimizes the cosine response. To reduce the nadir FOV contamination (i.e. sky irradiance and for canopy irradiance) due to the hemispherical view of the sensor the instrument was placed on a 1.5 m long horizontal arm at a height of 1.5 m above the ground. To avoid the zenithal FOV contamination, the measurements were taken at least at a 15 m distance from the eddy covariance tower (maximum height of the tower was 6 m). The vegetation irradiance (sensor pointing nadir) and sky irradiance (sensor pointing zenith) were measured by rotating the spectroradiometer alternately to acquire spectra from the vegetation and from the sky. Hemispherical reflectance was derived as the ratio of reflected to incident radiance. Each reflectance spectrum was automatically calculated and stored by the spectroradiometer as an average of 20 readings. Before starting each spectral sampling, a dark current measurement was done. For more details on experimental set-up see Vescovo et al. (2012). Spectral measurements were collected from spring until the cutting date at Amplero and Monte Bondone, while at the site in Neustift, which is cut three times during the season, spectral measurements were taken about once per week throughout the growing season of 2006.

2.3 Biophysical and biochemical canopy properties

Samples for dry phytomass, nitrogen and water content measurements were collected at the time of the hyperspectral measurements in the field of view of the hyperspectral sensor (see Vescovo et al. 2012 for more details). A similar dataset was collected in 2013 at Monte Bondone by combining hyperspectral data with chlorophylls measurements. Chlorophylls samples were collected in the field of view of the hyperspectral sensor and chlorophylls content was detected by UV-VI spectroscopy. First, the samples were grinded in presence of liquid nitrogen and then immersed in 80% acetone solution (0.1 g per 10 ml), shaken for 10 min in an automatic shaker at 250 rpm (Universal Table Shaker 709), and centrifuged at 4000 rpm for 10 min (Eppendorf 5810 R) in order to remove particles from the solution. The absorbance of extracted solutions was measured at 470, 646.8 and 663.2 nm by a UV/VIS spectrophotometer (Shimadzu UV-1601), and the concentrations of chlorophyll a (C_a), chlorophyll b (C_b) and carotenoids (C_{x+c}) were calculated as proposed by Lichtenthaler (1987). The weight of sampled sediment was used to calculate pigments concentrations per unit leaf mass (mg g^{-1}) and the weight of green biomass per ground area was used to obtain the total chlorophylls content (mg m^{-2}).

2.4 CO_2 flux measurements

Continuous measurements of the net ecosystem CO_2 exchange (NEE) were made by the eddy covariance (EC) technique (Baldocchi et al., 1996; Aubinet et at., 2012) at the six study sites using identical instrumentation. The three wind components and the speed of sound were measured using ultra-sonic anemometers, and CO_2 molar densities using open-path infrared gas analyzers (IRGAs), as detailed in Tables ~~1~~S1 and S2 in the Supplement section. Raw data were acquired at 20 Hz and averaged over 30 min time windows in post-processing. Turbulent fluxes were obtained from raw data by applying block averaging (Monte Bondone, Neustift, validation sites) or linear de-trending (Amplero) methods with a time window of 30 minutes. A 3D coordinate correction was performed according to Wilczak et al. (2001). The CO_2 fluxes were corrected for the effect of air density fluctuations as proposed by Webb et al. (1980). Low- and high-pass filtering was corrected for following Aubinet et al. (2000) (Amplero, Monte Bondone) or Moore (1986) (Neustift, validation sites). Data gaps due to sensors malfunctioning or violation of the assumptions underlying the EC method were removed and filled using the gap-filling and

flux-partitioning techniques as proposed in Wohlfahrt et al. (2008). Ecosystem respiration (Reco) was calculated from the y-intercept of the light response model (see eq. 4). Gross primary productivity (GPP) was calculated as the difference between NEE and Reco. Half-hourly NEE and GPP values were averaged between 11:00 to 14:00 solar local time (at the time window of optical measurements) to allow for direct comparison with the hyperspectral data, and daily sums were also computed. At each site the following supporting environmental measurements were acquired: photosynthetically active radiation (PAR; quantum sensors), air temperature (Ta; PT100, thermistor and thermoelement sensors), and humidity (RH; capacitance sensors) at some reference height above the canopy, and soil temperature (Ts; PT100, thermistor and thermoelement sensors) and volumetric water content (SWC; dielectric and time-domain reflectometry sensors) in the main rooting zone. In this study we used CO_2 flux and meteorological data of the years 2005 and 2006 for Monte Bondone and of 2006 for the other sites.

2.5 Estimation of grassland ecophysiological parameters

Canopy light use efficiency (ε) was derived from photosynthetically active radiation (PAR) absorbed by the canopy (APAR) as:

$$\varepsilon = \frac{\mathrm{GPP}}{\mathrm{APAR}} = \frac{\mathrm{GPP}}{\mathrm{PAR}*\mathrm{fAPAR}} \quad (2)$$

and was estimated both at midday and daily time resolution. We estimated the fraction of PAR absorbed by the canopy (fAPAR) from measured values of the leaf area index (LAI) using the Lambert-Beer law:

$$fAPAR = 0.95\left(1 - e^{(-k\,LAI)}\right) \quad (3)$$

where k is the canopy extinction coefficient (fixed at k=0.4 as defined for southern mixed-grass prairie in Texas; Kiniry et al., 2007) and 0.95 is the proportion of intercepted PAR that is absorbed by plants (Schwalm et al., 2006). LAI was quantified non-destructively by an indirect method based on canopy PAR transmission using line PAR sensors (SunScan, Delta-T, UK) and inversion of a RTM (Wohlfahrt et al., 2001). These measurements were done within the footprint area of the spectroradiometer simultaneously with the hyperspectral measurements.

Three additional key parameters of the response of NEE to PAR were extracted by fitting measured NEE and PAR to a simple Michaelis-Menten-type model:

$$\mathrm{NEE} = \frac{-\alpha\ \mathrm{PAR} F_{sat}}{\alpha\ \mathrm{PAR} + F_{sat}} + R_{eco} \quad (4)$$

where α represents the apparent quantum yield (µmol CO_2 µmol photons^{-1}), F_{sat} the asymptotic value of GPP (µmol CO_2 m^{-2} s^{-1}), PAR the photosynthetically active radiation (µmol photons m^{-2} s^{-1}) and R_{eco} the ecosystem respiration (µmol CO_2 m^{-2} s^{-1}). For all sites, using the Levenberg-Marquardt (1963) algorithm the parameters of Eq. (4) were estimated by fitting Eq. (4) to both day and nighttime data, which were pooled into 3-day blocks centered on the date of the hyperspectral data acquisition. For each acquisition date, we then used Eq. (3) to derive GPP at an incident PAR of 1500 µmol m^{-2} s^{-1}, referred to as GPP_{max} in the following.

2.6 Hyperspectral data analysis

In order to explore the information content of the hyperspectral data for estimating CO_2 fluxes (i.e. midday/daily average of NEE and GPP) and ecophysiological parameters (i.e. α, ε and GPP_{max}), we performed a correlation analysis between spectral reflectance indices (independent variables) and these (dependent) variables. To this end, we derived spectral ratio (SR; Eq. (5)), spectral difference (SD; Eq. (6)) and normalized spectral difference (NSD; Eq. (6)) indices using all possible two-band (i and j) reflectance (ρ) combinations between 400 and 1000 nm (180600 combinations). These three formulations were selected since they represent the most common equations used to compute vegetation indices (see Table 2).

$$SR_{i,j} = \frac{\rho_i}{\rho_j} \quad (5)$$

$$SD_{i,j} = \rho_i - \rho_j \quad (6)$$

$$NSD_{i,j} = \frac{\rho_i - \rho_j}{\rho_i + \rho_j} \quad (7)$$

Linear regression analysis was performed among all possible wavelength-combinations for all three index-types (SR, NSD and SD) and the investigated dependent variables.

The performance of linear models in predicting dependent variables (i.e. carbon fluxes and ecophysiological parameters) was evaluated by the coefficient of determination (R^2) and root

mean square error (RMSE). The coefficients of determination (R^2) resulting from the linear models were visualized in correlograms as depicted in an exemplary fashion in Figure 1.

We also calculated four SR- and seven NSD-indices which are commonly used in relation to vegetation activity and CO_2 fluxes (Table 2). Figure 1 shows the location of these indices in the waveband space of the correlograms. In this analysis, we also considered the Enhanced Vegetation Index (EVI), which is one of the most frequently used vegetation index to predict CO_2 fluxes. In the Fig. 1 the location of EVI is not shown since this index is computed by the combination of three spectral bands as shown in Table 2.

The robustness of the model selected on the basis of the best band combinations for all ecophysiological parameters for each site and all sites pooled was tested by the leave-one-out cross-validation technique. The predictive performance was expressed as the cross-validated coefficient of determination (R^2_{CV}) and the cross-validated root mean square error ($RMSE_{CV}$). In addition, the capability of the selected models in predicting different ecophysiological parameters was tested by applying the selected models to the validation dataset (Table S2) composed by three different grasslands not used in the previous analysis. This dataset was selected because the hyperspectral and flux data were collected by using exactly the same protocol applied for the main dataset (see sect.2.1).

In order to explore the basis of the correlation between the selected band combinations and ecophysiological variables (e.g. α, GPP_{max}, GPP, ε) the relationship between the selected bands and biophysical parameters such as dry phytomass, nitrogen and water content collected during the field campaign in the same footprint of the hyperspectral measurements was examined.

2.7 Band selection based on the combination of random forests and genetic algorithm (GA–rF)

In order to complement the more conventional analysis described in the previous section, we also explored the use of a hybrid feature selection strategy based on a genetic algorithm and random forests (GA–rF). The first method was used for the feature selection and the second one as regression for predicting the target variables. First of all, the original dataset was aggregated to 10 nm bands in order to reduce the effects of autocorrelation in frequency space. The algorithm generates a number of possible model solutions (chromosomes) and uses these to evolve towards

an approximation of the best solution of the model. In our case the genes of each chromosome correspond to the wavebands. We made use of 5 genes for each chromosome in order to overcome overfitting. Each population of 1000 chromosomes evolved for 200 generations. The mutation chance was set to the inverse of population size increased by one. The fitness of each chromosome was measured by applying the random forest algorithm (Breiman, 2001). This was used as an ensemble method for regression that is based on the uncontrolled development of decision trees (n=100). We opted for this method because of its demonstrated efficiency with large datasets. In combining the two methods we choose the mean squared error as the target variable to be minimized.

3 Results

3.1 Seasonal variation of meteorological variables, LAI and CO_2 fluxes

Environmental conditions and the seasonal development of LAI, NEE, GPP α, ε and GPP_{max} during the study period are shown in Figure 2. A strong influence of the typical climatic conditions at the three study sites ~~is~~ was evident: Amplero was characterized by a Mediterranean climate, with highest incoming radiation and temperatures, and the lowest amount of precipitation which translated into a substantial seasonal drawdown of soil moisture~~;~~. Monte Bondone and Neustift, more influenced by continental Alpine climate, experienced comparably lower temperatures with higher precipitation and soil moisture with respect to Amplero (Fig. 2).

Maximum LAI values were similar at Monte Bondone and Amplero (2.8-3.4 m^2 m^{-2}), while, twice as much leaf area developed at the more intensively managed study site Neustift~~,~~. ~~which~~ The latter was also characterized by higher NEE and GPP (i.e. more photosynthesis and net uptake of CO_2). The reductions in leaf area associated with the cuts of the grasslands were associated as expected with marked increases and reductions in NEE and GPP, respectively. The canopy light use efficiency, ε, was inversely related to GPP and LAI, peaking at the beginning of the season at Amplero and Monte Bondone (0.01-0.10 µmol photons µmol CO_2^{-1}), while for Neustift ε showed the highest values after the cuts (0.01-0.20 µmol photons µmol CO_2^{-1}). At Amplero, α and GPP_{max} peaked in spring and then decreased during the summer drought period,

while at Neustift and Monte Bondone, temporal patterns of α and GPP_{max} were more strongly affected by management.

3.2 Hyperspectral data and their relation to CO_2 fluxes and ecophysiological parameters

~~Figure 3 reports key spectral signatures of the grasslands collected during the study period. The reflectances in the NIR region decreased (NIR; 700–1000 nm) and increased in the blue region (420–540 nm) from early to late spring until the harvest for the Mediterranean grassland of Amplero (Fig. 3a) (Balzarolo, 2008). This is a typical trend for Mediterranean grasslands characterized by leaf senescence due to drought conditions (Fava et al., 2007; Vescovo et al. 2012). For Monte Bondone in 2006 and Neustift (Fig. 3b, d) the reflectance in the green (540–580 nm) and NIR region increased and decreased in the visible region with increasing LAI and phytomass.~~

Figures 3-5 show correlograms between NSD-, SR- and SD-type indices, respectively, and the investigated dependent midday ecophysiological parameters and fluxes. The correlograms for daily data can be found in the Supplement (Figures S2-S4). Selected examples of key spectral signatures of the investigated grasslands are shown in Figure S1 in the Supplementary material.

A number of interesting insights may be gained from Figures 3-5 and Figures S2-S4, which we summarize in the following:

(i) The correlograms exhibited quite different patterns – some correlograms showed that a wide range of band combinations was able to explain the simulated quantities (e.g. GPP at Amplero; Fig. 3; Fig. S2), while some correlograms exhibited very pronounced patterns, with the R^2 value changing greatly with subtle changes in band combinations (e.g. ε at Neustift; Fig. 3; Fig. S2).

(ii) Maximum R^2 values were often clearly higher than the surrounding areas of high predictive power (e.g. ε at Amplero; Fig. 3).

(iii) The different types of indices (compare Figs. 3-5) yielded similarly high correlations with the same dependent variable at the same site in similar spectral regions~~,~~. This indicat~~esing~~ that band selection is more important for explanatory power than the mathematical

formulation of the VI (i.e. ratio *vs.* difference, with/without normalization). SR and NSD indices (Figs. 3 and 4) yielded similar results compared to SD indices (Fig. 5).

(iv) The highest correlations for all dependent variables were found either for indices combining bands in the visible range (VIS: <700 nm) or the red edge and NIR (NIR: >700 nm), corresponding to spectral regions used by indices such as the SRPI, NPCI, PRI and NPQI, and the CI and WI, respectively. Spectral regions of well-known indices, such as NDVI, SR, SIPI or GRI, which exploit the contrasting reflectance magnitudes in the visible and NIR (Fig. S1), resulted in comparably lower correlations.

(v) For midday and daily time resolutions different band combinations were selected (e.g. NEE at Amplero; compare Figs. 4 and S3). For similar selected regions, daily averages were characterized by higher explanatory power compared to midday averages (e.g. ε at Neustift).

Figure 6 shows the performance of linear regression models for the best NSD-type indices for midday ecophysiological parameters for each site and all sites pooled (Figure S7 in the Supplement shows the results of the same analysis for daily averages). Large differences existed between the study sites in the explanatory power of the same index for the same dependent variable. The highest R^2cv and values were generally obtained for Amplero, followed by Neustift and then Monte Bondone and the lowest R^2cv values resulted when data from all three sites were pooled, confirming the difficulties in finding a general relation valid among sites.

For Amplero and Neustift the NIR vs. NIR combinations showed a positive linear regression model with α, GPP_{max} and GPP, while for Monte Bondone a negative linear correlation was observed. For Amplero the VIS vs. VIS combination showed a good performance in predicting ε; the NIR vs. NIR combinations showed good performance for Neustift and VIS vs. NIR combination for Monte Bondone. The linear models for NEE were site-specific. In fact, Amplero and Monte Bondone showed a positive linear regression model for NEE but the VIS vs. VIS band combination was selected for Amplero and NIR vs. NIR combination for Monte Bondone. Neustift performed well with NEE for NIR vs. NIR combinations, but with an inverse relationship.

The different type of indices (compare Figs. 6, S5 and S6) resulted in similar models. The different time resolutions gave different models (e.g. GPP, ε and NEE at Monte Bondone, compare Figs. 6 and S7 or Figs. S5 and S8 or Figs. S6 and S9).

3.3 Correlation between conventional VIs, ecophysiological variables and CO_2 fluxes

The correlation analysis between the conventional VIs, the midday CO_2 fluxes (Table 3) and ecophysiological parameters (Table 4), generally confirmed the results obtained with the hyperspectral data.

For the same dependent variable (α, GPP_{max}, GPP, ε and NEE), the performance of the various VIs showed large differences between sites. For example, for GPP_{max} all of the investigated indices except NPQI resulted in significant linear correlations at Amplero, explaining 41-89% of the variability in GPP_{max}. In contrast, only NDVI, PRI, NPCI and SRPI showed a slightly significant linear performance (17-26%) for GPP_{max} at Neustift.

The different VIs performed differently in predicting the same dependent variable at the different study sites. For all dependent variables (Tables 3, 4 and S3), the VI resulting in the highest R^2 values was never the same at all sites. Often the best fitting VI at one site resulted in a non-significant correlation at another site. Therefore, none of the dependent variables clearly emerged as the one best predicted (Tables 3, 4 and S3).

When data from all sites were pooled, models showed the same performance for the same VI and dependent variable except for GPP and NEE. The best performing VI for GPP and NEE was SIPI, NPCI performed best for α , GRI for ε, SIPI for GPP_{max}.

The choice of the averaging period (midday *vs*. daily) applied to ε, NEE and GPP did generally not modify the ranking of the VIs, but the R^2 values tended to be similar or somewhat higher at the daily time scale (compare Tables 3 and 4 with Table S3).

3.4 Evaluation of the model performance

Figure 7 shows the results of the validation for each ecophysiological parameter and midday averaged fluxes and NSD-, SR- and SD-type indices against data from the validation sites. The

models used in the validation are based on the best models determined for each site (i.e. Amplero, Neustift and Monte Bondone) and by pooling together the two alpine grasslands of Monte Bondone and Neustift (referred to as M.Bondone&Neustift).

Overall, the results of the validation were mixed. Good performance was observed mainly for the Neustift, Monte Bondone and pooled M.Bondone&Neustift models (see Table S4 in the Supplement section). In particular, the best performance values were obtained for: (i) α for the pooled Monte Bondone and Neustift model for SR-type indices; (ii) GPP_{max} for NSD-, SR- and SD-type indices and models except for Amplero; and (iii) for midday GPP for all NSD-, SR-, and SD-type indices and models. It is interesting to note that lower performances were generally found for the models based on the Amplero parameterization. This is understandable as Monte Bondone and in particular Neustift were structurally and functionally much more similar to the validation sites compared to Amplero (Tables 1 and S2). Considerably poorer performance was observed for ε and NEE across all model-index type combinations (Table S4). The validation at daily time scale always resulted in a poorer performance compared to the midday average time scale (Fig. S10 and Table S5 in the Supplement section).

3.5 Effects of canopy structure on selected band combinations

Tables 5 and S6 show the results of the correlation analysis between the selected models for ecophysiological variables and fluxes and biophysical properties of vegetation such as dry phytomass, nitrogen and water content. Overall, the spectral response in the selected band combinations for NSD, SR and SD-type indices was strongly related to vegetation properties of the three grasslands (e.g. nitrogen and dry phytomass) which impacted on their spectral response in the NIR and VIS regions. For the Mediterranean site (Amplero) and for all eco-physiological parameters (i.e. α, GPP_{max}, GPP, ε), dry phytomass was the main driving factor of the spectral response in the selected bands, while nitrogen content drove the spectral response in the NIR region for Neustift. For Monte Bondone, both dry phytomass and nitrogen content affected the spectral response of the grassland. Similar results were obtained for SR- and SD-type indices.

Figs. 8 and S11 in the Supplement show the correlation analysis between the selected bands for NSD-, SR- and SD-type indices and chlorophylls content for Monte Bondone in 2013. The chlorophylls content showed a very good correlation for all selected models and for all indices.

The values of R^2 were always higher than the values of R^2 obtained for the other biophysical variables (Tables 5 and S6). In Figure 9, it is possible to see that, NSD- and SR-type indices for the selected bands for estimating GPP (i.e. 996 nm and 710 nm) are strongly correlated with canopy total chlorophyll content ($R^2 > 0.80$).

3.6 Band selection using GA-rF method

Figure 9 shows the results of the band selection based on GA–rF method. In particular, each plot represents the frequency of the occurrence of each band in the genetic algorithm.

Overall, using the GA-rF method it was possible to identify portions of the spectrum that were of particular significance for estimating specific properties of the different ecosystems. For example, for predicting midday GPP (Fig. 9b) for all sites pooled together, the bands at 430 nm, 630 nm, 660 nm and 710 nm showed the best results. The bands at 505 nm played an important role in predicting midday GPP for Amplero; bands at 660 nm for Neustift and bands 710 nm for Monte Bondone. Some differences were found for the different time resolutions (compare Figs. 9b and 9c). For example, the bands at 580 nm and 800 nm showed the best results for Amplero and bands at 530 nm for Neustift.

Figure 10 shows the results for the band selection by GA-rF methods for biophysical variables (i.e. dry phytomass, nitrogen and water content). For the variables related to slow processes the GA-rF method highlighted different bands for different sites; a much higher between site variability for the variables related to ecophysiological processes (e.g. ε, α and GPP_{max}) was detected and we weren't able to identify common "hot spots".

4 Discussion

This study aimed at evaluating the potential of hyperspectral reflectance measurements to simulate CO_2 fluxes and ecophysiological variables of European mountain grasslands over a range of climatic conditions and management practices (grazing, harvest). To this end, we combined eddy covariance CO_2 flux measurements with ground-based hyperspectral measurements at six mountain grassland sites in Europe.

Up-scaling of in-situ relationships between VI indices and CO_2 fluxes and ecophysiological parameters

Despite the fact that we focused on a single type of ecosystem, our results showed that large differences existed among the investigated sites in the relationships between hyperspectral reflectance data and CO_2 fluxes and ecophysiological parameters. For all study sites pooled, hyperspectral reflectance data explained 40-68% of the variability in the dependent variables (Figs. 3-5). The conventional VIs yielded a maximum of 47% of explained variability in the data (Tables 3-4).

This is the first study comparing different grasslands characterized by different plant species and environmental conditions. The use of simple models based on a linear relationship between GPP and VIs, related to canopy greenness, has proven to be a good proxy for GPP of ecosystems with strong green-up and senescence (Peng et al., 2011; Rossini et al., 2012). The loss of this relationship may be related to low ε variability due to abiotic and biotic stressors, the dependency of PRI on LAI, leaf and canopy biochemical structure (e.g. leaf orientation), and xanthophyll cycle inhibition or saturation and zeaxanthin-independent quenching (Gamon et al., 2001; Filella et al., 2004; Rahimzadeh-Bajgiran et al. 2012; Hmimina et al., 2014). For alpine grasslands, a key meteorological variable that played a relevant role in stimulating ε was high soil water content associated with low temperatures (Polley et al. 2011). Low soil water contents triggered a decrease in leaf conductance as well as in ε and in α also for two oak and beech ecosystems (Hmimina et al., 2014). However, no significant differences in leaf biochemical and structural properties of the canopy at lowest and highest water content were found. In addition, in this special issue, Sakowska et al. (2014) showed that ε is also strongly affected by the directional distribution of incident PAR, i.e. the ratio of direct to diffuse PAR.

Considering all sites pooled together (Figs. 3 and S2), NSD-type indices showed a very poor correlation in the VIS vs. NIR band combinations (i.e. traditional "greenness" indices, see Table 2) with GPP. It is well-known in the literature (Rossini et al., 2010, 2012; Peng et al., 2010; Sakowska et al., 2014) that “greenness” indices, for grasslands and crops, are often good proxies of fAPARgreen (and thus carbon fluxes). Interestingly, in our study their performance was considerably poorer than expected. The NSD-type index showed a better performance in VIS vs. VIS band combinations than VIS vs. NIR ones. VIS vs. VIS band combination for NSD-type

indices (e.g. green vs. blue or red, green vs. green wavelengths; see e.g. Inoue et al, 2008) are defined as "greenness" indices (Fig. 1), although their performance is generally much poorer than NSD VIS vs. NIR indices. These results are likely due to the confounding effects of the different canopy structures, and consequently of the different NIR response of the investigated grasslands (see Fig. S1). In fact, the different grassland structures (spatial distribution of photosynthetic, and also non photosynthetic material, leaf angles, etc.) is affecting our ability to use traditional indices to estimate fAPARgreen (and fluxes) when we consider different grasslands together because the structural effects on scattering are very complex in the NIR (Jacquemoud et al., 2009; Knyazikhin et al., 2012). These results are of importance for the community, which still relies a lot on these relationships, also favoured by the availability of affordable narrow-band sensors that allow continuous monitoring of e.g. NDVI. These results suggest that waveband combinations not exploited by presently used (conventional) VIs may offer considerable potential for predicting grassland CO_2 fluxes, which has implications for the design and capabilities of future space/airborne or ground-based low cost sensors. In particular, these results also have a strong impact on our ability to up-scale grassland fAPARgreen and carbon fluxes using upcoming sensors (e.g. Sentinel 2).

The evaluation of the models found for the main dataset against three new sites ~~confirme~~ showed that at least some of these models can be transferred to predict carbon fluxes and ecophysiological parameters for similar grasslands (Fig. 7). However, for some parameters (e.g. ε), the independent validation indicated a poor performance, it ~~these findings also~~ challenges the current practice in up-scaling to larger regions by grouping all grasslands into a single plant functional type (PFT). We advocate more studies to be conducted merging CO_2 flux with hyperspectral data by means of models which use a more process-oriented and coupled approach to simulating canopy CO_2 exchange and reflectance in order to explore the causes underlying the observed differences between seemingly closely related study sites.

Grassland structural characteristic and their spectral response

Although we considered similar ecosystems (belonging to the same vegetation type) the investigated canopies were very different and included Mediterranean, extensive alpine and intensive alpine grasslands with very different canopy structures in terms of leaf orientation,

amount and spatial distribution of green and non-photosynthetic components, leaf nitrogen and water content as detailed in Vescovo et al. (2012).

For Amplero and Neustift NSD-type indices performed well for NIR vs. NIR band combinations for all investigated parameters, while Monte Bondone showed best performances in the VIS vs. NIR band combinations for GPP_{max} and ε (Fig. 6). The dry phytomass was the main driving factor of the spectral response in NIR vs. NIR band combinations for Amplero, while nitrogen content drove the spectral response in NIR vs. NIR band combinations of Neustift for all parameter except for α (Tab. 5 and S6). Interestingly, for Monte Bondone both dry phytomass and nitrogen content explained the spectral response of the grassland in VIS vs. NIR band combinations for GPP_{max} and ε while no significant relationships with biophysical variables were found for α, GPP, NEE. These results partially confirm the findings of Vescovo et al. (2012), who highlighted a strong relationship, for several grassland types, between an NSD-type index and phytomass.

For Monte Bondone, NSD- and SR-type indices for the selected bands for estimating all variables except α were strongly correlated with canopy total chlorophyll content ($R^2 > 0.85$).

The chlorophyll indices (e.g. RedEdge NDVI and CI; see Tables 3 and 4) – which are considered the best indices for estimating carbon fluxes on grasslands and crops) – showed in our dataset a good performance for Amplero and Monte Bondone, but performed poorly for Neustift.

It was demonstrated by many authors that the red edge domain, where reflectance changes from very low in the absorption region to high in the NIR, is one of the best descriptors of chlorophyll concentration. On the other hand, it is well known that the canopy structure can be a very strong confounding factor. Our results confirm that this topic needs to be further investigated, as this finding has a relevant impact concerning the use of Sentinel 2 to upscale fAPAR and carbon flux observations.

It is interesting to see that the NSD-type indices in the NIR vs. NIR band combinations appeared to be the best proxy for GPP fluxes when all the grasslands were pooled together. These results can be linked to the controversial paper focused on the strong impact of structure on the ability to estimate canopy nitrogen content (Knyazikhin et al., 2012) and confirm the need for more studies in this direction. Good relationships were found between the NIR vs. NIR band

combinations (>750nm wavelengths) and fluxes; the physical basis of these relationships needs to be further investigated. In fact, it is important to highlight that the literature indicates that the wavelengths in the NIR (>750nm) are not sensitive to chlorophyll content, but they are related to leaf, canopy structure, and -around the 970nm area- to water.

As confirmed by comparing the correlation matrix approach with the GA-rF approach we couldn't find a universal relationship between reflectance in specific wavelengths of the light spectrum to biophysical properties of vegetation. We think that this is strongly linked to vegetation structure effects. For this reason we believe that further research for disentangling the impact of factors like bidirectional reflectance distribution function and scaling effects is necessary.

5 Conclusions

The present study focused on understanding the potential of hyperspectral VIs in predicting grassland CO_2 exchange and ecophysiological parameters (α, ε and GPP_{max}) for different European mountain grasslands.

The major finding of this study is that the relationship between ground-based hyperspectral reflectance and the ecosystem-scale CO_2 exchange of mountain grasslands is much more variable than what might be supposed given this closely related group of structurally and functionally similar ecosystems. As a consequence, the unique models of mountain grassland CO_2 exchange, i.e. the best fitting models for all sites pooled, explained 47% and 68% of the variability in the independent variables when established VIs and optimized hyperspectral VIs, respectively, were used. Interestingly, VIs based on reflectance either in the visible or NIR part of the electromagnetic spectrum were superior in predicting mountain grassland CO_2 exchange and ecophysiological parameters compared to commonly used VIs which are based on a combination of these two wavebands. The band selection based on GA-rF algorithm confirmed that is difficult to define a universal band range able to describe ecophysiological parameters, carbon fluxes and biophysical variables even for a closely related group of ecosystems.

The take-home message from this study thus is that continuing efforts are required to better understand differences in the relationship between ecosystem-scale reflectance and CO_2

exchange and to improve models of this relationship which can be employed to up-scale the land CO_2 exchange to larger spatial scales based on optical remote sensing data. Initiatives such as SpecNet (http://specnet.info; Gamon et al., 2006), the COST Action ES0903 (EUROSPEC; http://cost-es0903.fem-environment.eu/) and the COST Action ES1309 (OPTIMISE; http://www.cost.eu/domains_actions/essem/Actions/ES1309) are instrumental to this end as they provided the scale-consistent combination of hyperspectral reflectance and CO_2 exchange data.

Acknowledgements

MB acknowledges the support by the Methusalem program of the Flemish Government. LV and DG acknowledge the financial support obtained by the EU project CARBOEUROPE-IP (GOCE-CT-2003-505572) and the CARBOITALY project funded by the Italian Government. GW and AH acknowledge financial support by the Austrian National Science Fund (FWF) through grant agreements P17562 and P26425 and the Tyrolean Science Fund through grant agreement UNI-404/33. AH was financially supported through a DOC fellowship by the Austrian Academy of Sciences (ÖAW). ET acknowledges the support of the Province of Bolzano/Bozen through the project MONALISA. Article processing charges of this paper were covered by the EuroSpec COST action (ES0903).

References

Aubinet, M., Vesala, T., and Papale, D.: Eddy Covariance - A Practical Guide to Measurement and Data Analysis, Springer, ISBN: 978-94-007-2351-1, 2012.

Aubinet, M., Grelle, A., Ibrom, A., Rannik, U., Moncrieff, J., Foken, T., Kowalski, P., Martin, P., Berbigier, P., Bernhofer, C., Clement, R., Elbers, J., Granier, A., Grunwald, T., Morgenster, K., Pilegaard, K., Rebmann, C., Snijders, W., Valentini, R., and Vesala, T.: Estimates of the annual net carbon and water exchange of Europeran forests: the EUROFLUX methodology, Adv.Ecol.Res., 30, 113–75, 2000.

Bacour, C., Baret, F., and Jacquemoud, S.: Information content of HyMap hyperspectral imagery, Proceedings of the 1st International Symposium on Recent Advances in Quantitative Remote Sensing, Valencia (Spain), 503−508, 2002.

Bacour, C., Jacquemoud, S., Leroy, M., Hautecoeur, O., Weiss, M., Prévot, L., Bruguier, L., Chauki H.: Reliability of the estimation of vegetation characteristics by inversion of three canopy reflectance models on airborne POLDER data, Agronomie, 22, 555−565, 2002.

Baldocchi, D., Valentini, R., Running, S., Oechel, W., and Dahlman, R.: Strategies for measuring and modelling carbon dioxide and water vapour fluxes over terrestrial ecosystems, Glob. Change Biol., 2, 159–168, 1996.

Balzarolo, M.: Biometric parameters and fluxes estimations in Mediterranean mountainous grassland with remote sensing techniques, PhD thesis, University of Tuscia, 2008.

Balzarolo, M., Anderson, K., Nichol, C., Rossini, M., Vescovo, L., Arriga, N., Wohlfahrt, G., Calvet, J.-C., Carrara, A., Cerasoli, S., Cogliati, S., Daumard, F., Eklundh, L., Elbers, J. A., Evrendilek, F., Handcock, R. N., Kaduk, J., Klumpp, K., Longdoz, B., Matteucci, G., Meroni, M., Montagnani, L., Ourcival, J.-M., Sanchez-Canete, E. P., Pontailler, J.-Y., Juszczak, R., Scholes, B., and Pilar Martin, M.: Ground-based optical measurements at European flux sites: a review of methods, instruments and current controversies, Sensors, 11, 7954–7981, 2011.

Baret, F., Jacquemoud, S., Guyot, G., and Leprieur, C.: Modeled analysis of the biophysical nature of spectral shifts and comparison with information content of broad bands, Remote Sens. Environ., 41, 133−142, 1992.

Barnes, J. D., Balaguer, L., Manrique, E., Elvira, S., and Davison, A. W.: A reappraisal of the use of DMSO for the extraction and determination of chlorophylls a and b in lichens and higher plants, Environ. Exp. Bot., 32, 85–100, 1992.

Beer, C., Reichstein, M., Tomelleri, E., Ciais, P., Jung, M., Carvalhais, N., Rodenbeck, C., Arain, M. A., Baldocchi, D., Bonan, G. B., Bondeau, A., Cescatti, A., Lasslop, G., Lindroth, A., Lomas, M., Luyssaert, S., Margolis, H., Oleson, K. W., Roupsard, O., Veenendaal, E., Viovy, N., Williams, C., Woodward, F. I., and Papale, D.: Terrestrial gross carbon dioxide uptake: global distribution and covariation with climate, Science, 329, 834–838, doi:10.1126/science.1184984, 2010.

Breiman, L., Random Forests, Mach. Learn., 45, 5-32, 2001.

Cernusca, A., Bahn, M., Berninger, F., Tappeiner, U., Wohlfahrt, G.: Effects of land-use changes on sources, sinks and fluxes of carbon in European mountain grasslands, Ecosystems, 11:1335–1337, 2008.

Ciais, P., Wattenbach, M., Vuichard, N., Smith, P., Piao, S. L., Don, A., Luyssaert, S., Janssens, I. A., Bondeau, A., Dechow, R., Leip, A., Smith, P. C., Beer, C., van der Werf, G. R., Gervois, S., Van Oost, K., Tomelleri, E., Freibauer, A., Schulze, E. D., and Team, C. S.: The european carbon balance. Part 2: Croplands, Glob. Change Biol., 16, 1409–1428, 2010.

Clevers, J. G. P. W., Kooistraa, L., and Schaepman, M.E.: Estimatingcanopy water content using hyperspectral remote sensing data, Int. J. Appl. Earth Observ. Geoinform., 12, 119−125, 2010.

Clevers, J. G. P. W. and Gitelson, A. A.: Remote estimation of crop and grass chlorophyll and nitrogen content using red-edge bands on Sentinel-2 and -3, Int. J. Appl. Earth Obs., 23, 10 344–351, doi:10.1016/j.jag.2012.10.008, 2013.

Colombo, R., Meroni, M., Marchesi, A., Busetto, L., Rossini, M., Giardino, C., and Panigada, C.: Estimation of leaf and canopy water content in poplar plantations by means of hyperspectral indices and inverse modeling, Remote Sens. Env., 112, 4, 1820-1834, 2008.

Coops, N. C., Hilker, T., Hall, F. G., Nichol, C. J., and Drolet, G. G.: Estimation of light-use efficiency of terrestrial ecosystem from space: a status report, Bioscience, 60, 788–797, 2010.

Drolet, G. G., Huemmrich, K. F., Hall, F. G., Middleton, E. M., Black, T. A., Black, T., Barr, A., Barr, A. A., and Margolis, H.: A MODIS-derived photochemical reflectance index to detect interannual variations in the photosynthetic light-use efficiency of a boreal deciduous forest, Remote Sens. Environ., 98, 212–224, doi:10.1016/j.rse.2005.07.006, 2005.

EEA, Agriculture and environment in EU-15. The IRENA Indicator Report, EEA, Copenhagen, ISBN 92-9167-779-5, 2005.

Fava, F., Colombo, R., Bocchi, S., Meroni, M., Sitzia, M., Fois, N., and Zucca, C.: Identification of hyperspectral vegetation indices for Mediterranean pasture characterization, Int. J. Appl. Earth Obs. Geoinf., 11, 233–243, 2009.

Filella, I., Peñuelas, J., Llorens, L., and Estiarte, M.: Reflectance assessment of seasonal and annual changes in biomass and CO2 uptake of a Mediterranean shrubland submitted to experimental warming and drought. Remote Sens. Env., 90, 308–318, 2004.

Frankenberg, C., Fisher, J. B., Worden, J., Badgley, G., Saatchi, S. S., Lee, J.-E., Toon, G. C., Butz, A., Jung, M., Kuze, A., and Yokota, T.: New global observations of the terrestrial carbon cycle from GOSAT: patterns of plant fluorescence with gross primary productivity, Geophys. Res. Lett., 38, L17706, doi:10.1029/2011gl048738, 2011.

Gamon, J. A., Peñuelas, J., and Field, C. B.: A narrow-waveband spectral index that tracks diurnal changes in photosynthetic efficiency, Remote Sens. Environ., 41, 35–44, 1992.

Gamon, J. A., Field, C. B., Fredeen, A. L., and Thayer, S.: Assessing photosynthetic downregulation in sunflower stands with an optically-based model. Plant Biology 67, 113–125, 2001.

Gamon, J. A., Rahman, A. F., Dungan, J. L., Schildhauer, M., Huemmrich, K. F.: Spectral Network (SpecNet): What Is It and Why Do We Need It?, Remote Sens. Environ. 103, 227-235, 2006.

Gamon, J. A., Coburn, C., Flanagan, L. B., Huemmrich, K. F., Kiddle, C., Sanchez-Azofeifa, G. A., Thayer, D. R., Vescovo, L., Gianelle, D., Sims, D. A., Rahman, A. F., and Pastorello, G. Z.: SpecNet revisited: bridging flux and remote sensing communities, Can. J. Remote Sens., 36, S376–S390, 2010.

Garbulsky, M. F., Peñuelas, J., Gamon, J., Inoue, Y., and Filella, I.: The photochemical reflectance index (PRI) and the remote sensing of leaf, canopy and ecosystem radiation use efficiencies –a review and meta-analysis, Remote Sens. Environ., 115, 281–297, 2011.

Gianelle, D., Vescovo, L., Marcolla, B., Manca, G., and Cescatti, A.: Ecosystem carbon fluxes and canopy spectral reflectance of a mountain meadow, Int. J. Remote Sens., 30, 435–449, 2009.

Gilmanov, T. G., Soussana, J. F., Aires, L., Allard, V., Ammann, C., Balzarolo, M., Barcza, Z., Bernhofer, C., Campbell, C. L., Cernusca, A., Cescatti, A., Clifton-Brown, J., Dirks, B. O. M., Dore, S., Eugster, W., Fuhrer, J., Gimeno, C., Gruenwald, T., Haszpra, L., Hensen, A., Ibrom, A., Jacobs, A. F. G., Jones, M. B., Lanigan, G., Laurila, T., Lohila, A., Manca, G., Marcolla, B., Nagy, Z., Pilegaard, K., Pinter, K., Pio, C., Raschi, A., Rogiers, N., Sanz, M. J., Stefani, P., Sutton, M., Tuba, Z., Valentini, R., Williams, M. L., and Wohlfahrt, G.: Partitioning European

grassland net ecosystem CO_2 exchange into gross primary productivity and ecosystem respiration using light response function analysis, Agr. Ecosyst. Environ., 121, 93–120, 2007.

Gitelson, A. A., and Merzlyak, M. N.: Remote estimation of chlorophyll content in higher plant leaves. Int. J. Remote Sens., 18, 2691–2697, 1997.

Gitelson, A. A., Viña, A., Ciganda, V., Rundquist, D. C., and Arkebauer, T. J.: Remote estimation of canopy chlorophyll content in crops, Geophys. Res. Lett., 32, L08403, doi:10.1029/2005GL022688, 2005.

Gitelson, A. A., Viña, A., Rundquist, D. C., Arkebauer, T. J., Keydan, G., Leavitt, B., Ciganda, V., Burba, G. G., and Suyker, A. E.: Relationship between gross primary production and chlorophyll content in crops: Implications for the synoptic monitoring of vegetation productivity, Geophys. Res. Lett., 111, D08S11. http://dx.doi.org/ 10.1029/2005JD006017, 2006.

Gitelson, A.A., Vina, A., Masek, J.G., Verma, S. B., and Suyker, A.E.: Synoptic monitoring of gross primary productivity of maize using Landsat data, IEEE Geosci. Remote S., 5, 133–137, 2008.

Gitelson, A. A., Peng, Y., Masek, J. G., Rundquist, D. C., Verma, S., Suyker, A., Baker, J. M., Hatfield, J. L., and Meyers, T.: Remote estimation of crop gross primary production with Landsat data, Remote Sens. Environ., 121, 404–414, doi:10.1016/j.rse.2012.02.017, 2012.

Goerner, A., Reichstein, M., Tomelleri, E., Hanan, N., Rambal, S., Papale, D., Dragoni, D., and Schmullius, C.: Remote sensing of ecosystem light use efficiency with MODIS-based PRI, Biogeosciences, 8, 189–202, 2011.

Grossman, Y. L., Ustin, S. L., Sanderson, E., Jacquemoud, J., Schmuck, G., and Verdebout J.: Critique of stepwise multiple linear regression for the extraction of leaf biochemistry information from leaf reflectance data, Remote Sens. Environ., 56, 182–193, 1996.

Hatfield, J. L. Gitelson, A. A., Schepers, J. S., and Walthall, C. L.: Application of spectral remote sensing for agronomic decisions, Agron. J., 100,117–131, doi:10.2134/agronj2006.0370c, 2008.

Heinsch, F. A., Zhao, M. S., Running, S. W., Kimball, J. S., Nemani, R. R., Davis, K. J., Bolstad, P. V., Cook, B. D., Desai, A. R., Ricciuto, D. M., Law, B. E., Oechel, W. C., Kwon, H., Luo, H. Y., Wofsy, S. C., Dunn, A. L., Munger, J. W., Baldocchi, D. D., Xu, L. K., Hollinger, D. Y., Richardson, A. D., Stoy, P. C., Siqueira, M. B. S., Monson, R. K., Burns, S. P., and Flanagan, L. B.: Evaluation of remote sensing based terrestrial productivity from MODIS using regional tower eddy flux network observations, IEEE T. Geosci. Remote, 44, 1908–1925, 2006.

Hmimina, G., Dufrêne, E., and Soudani, K.: Relationship between photochemical reflectance index and leaf ecophysiological and biochemical parameters under two different water statuses: towards a rapid and efficient correction method using real-time measurements, Plant Cell Environ., 37, 473–487, 2014.

Inoue, Y., Peñuelas, J., Miyata, A., and Mano, M.: Normalized difference spectral indices for estimating photosynthetic efficiency and capacity at a canopy scale derived from hyperspectral and CO_2 flux measurements in rice, Remote Sens. Env., 112, 156–172, 2008.

Jacquemoud, S.: Inversion of the PROSPECT+SAIL canopy reflectance model from AVIRIS equivalent spectra: Theoretical study, Remote Sens. Environ., 44, 281–292, 1993.

Jacquemoud, S., Bacour, C., Poilvé, H., and Frangi, I.-P.: Comparison of four radiative transfer models to simulate plant canopies reflectance: direct and inverse mode, Remote Sens. Env., 74, 471–481, 2000.

Jordan, C. F.: Derivation of leaf area index from quality of light on the forest floor, Ecology, 50, 663–666, 1969.

Kiniry, J. R., Burson, B. L., Evers, G. W., Williams, J. R., Sanchez, H., Wade, C., Featherston, J. W., and Greenwade J.: Coastal bermudagrass, bahiagrass, and native range simulation for diverse sites in Texas, Agron. J., 99, 450–61, 2007.

Knyazikhin, Y., Schull, M. A., Stenberg, P., Mõttus, M., Rautiainen, M., Yang, Y., Marshak, A., Latorre Carmona, P., Kaufmann, R. K, Lewis, P., Disney, M. I., Vanderbilt, V., Davis, A. B., Baret, F., Jacquemoud, S., Lyapustin, A., and Myneni, R. B. : Hyperspectral remote sensing of foliar nitrogen content, Proc. Natl. Acad. Sci. USA, 110, 185–192, 2012.

Lambers, H., Chapin III, F. S., and Pons, T.L.: Plant physiological ecology, Springer-Verlag, Berlin, 540, 1998.

Li, L., Ustin, S. L., Riano, D.: Retrieval of fresh leaf fuel moisture content using genetic algorithm – partial least squares modeling (GA-PLS). EEE T. Geosci. Remote Letters, 4, 216–220, 2007.

Lichtenthaler, H. K: Chlorophylls and carotenoids: Pigments of photosynthetic biomembranes, Methods in Enzymology,148, 349-382, 1987.

Marquardt, D. W.: An Algorithm for Least-Squares Estimation of Nonlinear Parameters, SIAM J. Appl. Math., 11, 431–441, doi:10.1137/0111030, 1963.

Mauder, M., Foken, T., Bernhofer, C., Clement, R., Elbers, J., Eugster, W., Grünwald, T., Heusinkveld, B., and Kolle, O.: Quality control of CarboEurope flux data – Part 2: Inter-comparison of eddy-covariance software, Biogeosciences, 5, 451–462, 2008, http://www.biogeosciences.net/5/451/2008/.

Meroni, M., Rossini, M., Guanter, L., Alonso, L., Rascher, U., Colombo, R., and Moreno, J.: Remote sensing of solar induced chlorophyll fluorescence: review of methods and applications, Remote Sens. Environ., 113, 2037–2051, 2009.

Meroni, M., Barducci, A., Cogliati, S., Castagnoli, F., Rossini, M., Busetto, L., Migliavacca, M., Cremonese, E., Galvagno, M., Colombo, R., and Morra di Cella, U.: The hyperspectral irradiometer, a new instrument for long-term and unattended field spectroscopy measurements, Rev. Sci. Instrum. 82, 043106; 2011; http://dx.doi.org/10.1063/1.3574360.

Monteith, J. L.: Solar radiation and productivity in tropical tcosystems, J. Appl. Ecol., 9(3), 747–766, 1972.

Monteith, J. L. and Moss, C. J.: Climate and the Efficiency of Crop Production in Britain, Philos. Trans. R. Soc. London B Biol. Sci., 281, 277–294, doi:10.1098/rstb.1977.0140, 1977.

Moore, C.J.: Frequency response corrections for eddy correlation systems, Bound.-Lay. Meteorol., 37, 17–35, 1986.

Nichol, C. J., Lloyd, J., Shibistova, O., Arneth, A., Roser, C., Knohl, A., Matsubara, S., and Grace, J.: Remote sensing of photosynthetic-light-use efficiency of a Siberian boreal forest, Tellus B, 54, 677–687, 2002.

Ollinger, S. V., Richardson, A. D., Martin, M. E., Hollinger, D. Y., Frolking, S., Reich, P. B., Plourde, L. C., Katul, G. G., Munger, J.W., Oren, R., Smith, M.-L., Paw U, K. T., Bolstad, P. V., Cook, B. D., Day, M. C., Martin, T. A., Monson, R. K., and Schmid, H. P.: Canopy nitrogen, carbon assimilation, and albedo in temperate and boreal forests: functional relations and potential climate feedbacks, P. Natl. Acad. Sci. USA, 105, 19336–19341, doi:10.1073/pnas.0810021105, 2008.

Peng, Y., Gitelson, A. A., Keydan, G., Rundquist, D. C., and Moses, W.: Remote estimation of gross primary production in maize and support for a new paradigm based on total crop chlorophyll content, Remote Sens. Environ., 115, 978–989, 2011.

Peñuelas, J., Filella, I., Biel, C., Serrano, L., and Save, R.: The reflectance at the 950-970 nm region as an indicator of plant water status, Int. J. Remote Sens., 14, 1887–1905, 1993.

Peñuelas, J., Gamon, J. A., Fredeen, A., Merino, J., *and* Field, C. B., Reflectance indices associated with physiological changes in nitrogen- and water-limited sunflower leaves. Remote Sens. Environ., 48, 135–146, 1994.

Peñuelas, J., Filella, I., *and* Gamon, J. A.: Assessment of photosynthetic radiation-use efficiency with spectral reflectance, New Phytol., 131, 291–296, 1995.

Peñuelas, J., and Filella, I.: Visible and near-infrared reflectance techniques for diagnosing plant physiological status, Trends Plant Sci., 3, 151–156, 1998.

Peñuelas, J., Garbulsky, M. F., and Filella, I.: Photochemical reflectance index (PRI) and remote sensing of plant CO_2 uptake, New Phytol., 191, 596–599, 2011.

Polley, H. W., Phillips, B. L., Frank, A. B., Bradford, J. A., Sims, P. L., Morgan, J. A., and Kiniry, J. R.: Variability in light-use efficiency for gross primary productivity on Great Plains grasslands, Ecosystems, 14, 15–27, 2011.

Rahimzadeh-Bajgiran, P., Munehiro, M., and Omasa, K.: Relationships between the photochemical reflectance index (PRI) and chlorophyll fluorescence parameters and plant pigment indices at different leaf growth stages. Photosynt. Res., 113, 261–271, 2012.

Reichstein, M., Falge, E., Baldocchi, D., Papale, D., Valentini, R., Aubinet, M., Berbigier, P., Bernhofer, C., Buchmann, N., Gilmanov, T., Granier, A., Grünwald, T., Havrankova, K., Janous, D., Knohl, A., Laurela, T., Lohila, A., Loustau, D., Matteucci, G., Meyers, T., Miglietta, F., Ourcival, J.-M., Rambal, S., Rotenberg, E., Sanz, M., Seufert, G., Vaccari, F., Vesala, T., and Yakir, D.: On the separation of net ecosystem exchange into assimilation and ecosystem respiration: review and improved algorithm, Glob. Change Biol., 11, 1424–1439, 2005.

Riaño, D., Ustin, S. L., Usero, L., Patricio, M. A.: Estimation of fuel moisture content using neural networks. Lect. Notes in Comput. Sc., 3562: 489–498, 2005a.

Rossini, M., Meroni, M., Migliavacca, M., Manca, G., Cogliati, S., Busetto, L., Picchi, V., Cescatti, A., Seufert, G., and Colombo, R.: High resolution field spectroscopy measurements for estimating gross ecosystem production in a rice field, Agr. Forest Meteorol., 150, 1283–1296, 2010.

Rossini, M., Cogliati, S., Meroni, M., Migliavacca, M., Galvagno, M., Busetto, L., Cremonese, E., Julitta, T., C. Siniscalco, C., Morra di Cella, U., and Colombo, R.: Remote sensing-based estimation of gross primary production in a subalpine grassland, Biogeosciences, 9, 2565–2584, 2012.

Rouse, J. W., Haas, R. H., Schell, J. A., and Deering, D. W.: Monitoring vegetation systems in the Great Plains with ERTS. 3rd ERTS Symposium, NASA SP-351 I, 1973.

Sakowska, K., Vescovo, L., Marcolla, B., Juszczak, R., Olejnik, J., and Gianelle, D.: Monitoring of carbon dioxide fluxes in a subalpine grassland ecosystem of the Italian Alps using a multispectral sensor, Biogeosciences, 11, 4695-4712, doi:10.5194/bg-11-4695-2014, 2014.

Schotanus, P., Nieuwstadt, F. T. M., and De Bruin H. A. R.: Temperature measurement with a sonic anemometer and its application to heat and moisture fluxes, Bound. Lay. Meteorol., 26 81–93, 1983.

Schwalm, C. R., Black, T. A., Arniro, B. D., Arain, M. A., Barr, A. G., Bourque, C. P. A., et al.: Photosynthetic light use efficiency of three biomes across an East–west continental-scale transect in Canada, Agric. For. Meteorol., 140, 269–286, 2006.

Sims, D. A., and Gamon, J. A.: Relationships between leaf pigment content and spectral reflectance across a wide range of species, leaf structures, and developmental stages, Remote Sens. Env., 81, 337–354, 2002.

Soudani, K., Hmimina, G., Dufrêne, E., Berveiller, D., Delpierre, N., Ourcival, J.-M., Rambal, S., and Joffre, R.: Relationships between photochemical reflectance index and light-use efficiency in deciduous and evergreen broadleaf forests, Remote Sens. Env., 144, 73–84, 2014.

Soussana, J. F., Allard, V., Pilegaard, K., Ambus, C., Campbell, C., Ceschia, E., Clifton-Brown, J., Czobel, S., Domingues, R., Flechard, C., Fuhrer, J., Hensen, A., Horvath, L., Jones, M., Kasper, G., Martin, C., Nagy, Z., Neftel, A., Raschi, A., Baronti, S., Rees, R. M., Skiba, U., Stefani, P., Manca, G., Sutton, M., Tuba, Z., and Valentini, R.: Full accounting of the greenhouse gas (CO_2, N_2O, CH_4) budget of nine European grassland sites, Agri. Eco. Enviro., 121, 121–134, 2007.

Vescovo L., Wohlfahrt, G., Balzarolo, M., Pilloni, S., Sottocornola, M., Rodeghiero, M., and Gianelle, D.: New spectral vegetation indices based on the near-infrared shoulder wavelenghts fro remote sensign detection of grassland phytomass, Int. J. Remote Sens., 33, 7, 2012.

Waring, R., and Running, S. W.: Forest Ecosystems: Analysis at Multiple Scales, Elsevier, New York, 1998.

Webb, E. K., Pearman, G. I., and Leuning, R.: Correction of flux measurements for density effects due to heat and water vapour transfer, Q. J. Roy. Meteorol. Soc., 106, 85–100, 1980.

Vickers, D. and Mahrt, L.: Quality control and flux sampling problems for tower and aircraft data, J. Atmos. Oceanic. Tech., 14, 512–526, 1997.

Wilczak, J. M., Oncley, S. P., and Stage, S. A.: Sonic anemometer tilt correction algorithms, Bound.-Lay. Meteorol., 99, 127–150, 2001.

Wohlfahrt, G., Sapinsky, S., Tappeiner, U., and Cernusca, A.: Estimation of plant area index of grasslands from measurements of canopy radiation profiles, Agr. Forest Meteorol., 109, 1–12, 2001.

Wohlfahrt, G., Anderson-Dunn, M., Bahn, M., Balzarolo, M., Berninger, F., Campbell, C., Carrara, A., Cescatti, A., Christensen, T., Dore, S., Eugster, W., Friborg, T., Furger, M., Gianelle, D., Gimeno, C., Hargreaves, K., Hari, P., Haslwanter, A., Johansson, T., Marcolla, B., Milford, C., Nagy, Z., Nemitz, E., Rogiers, N., Sanz, M.J., Siegwolf, R. T. W., Susiluoto, S., Sutton, M., Tuba, Z., Ugolini, F., Valentini, R., Zorer, R., and Cernusca, A.: Biotic, abiotic and management controls on the net ecosystem CO_2 exchange of European mountain grasslands, Ecosystems, 11, 1338–1351, 2008.

Wohlfahrt, G., Pilloni, S., Hörtnagl, L., and Hammerle, A.: Estimating carbon dioxide fluxes from temperate mountain grasslands using broad-band vegetation indices, Biogeosciences, 7, 683–694, doi:10.5194/bg-7-683-2010, 2010.

Zarco-Tejada, P. J., Rueda, C. A., and Ustin, S. L.: Water content estimation in vegetation with MODIS reflectance data and model inversion method, Remote Sens. Env., 85, 109–124, 2003.

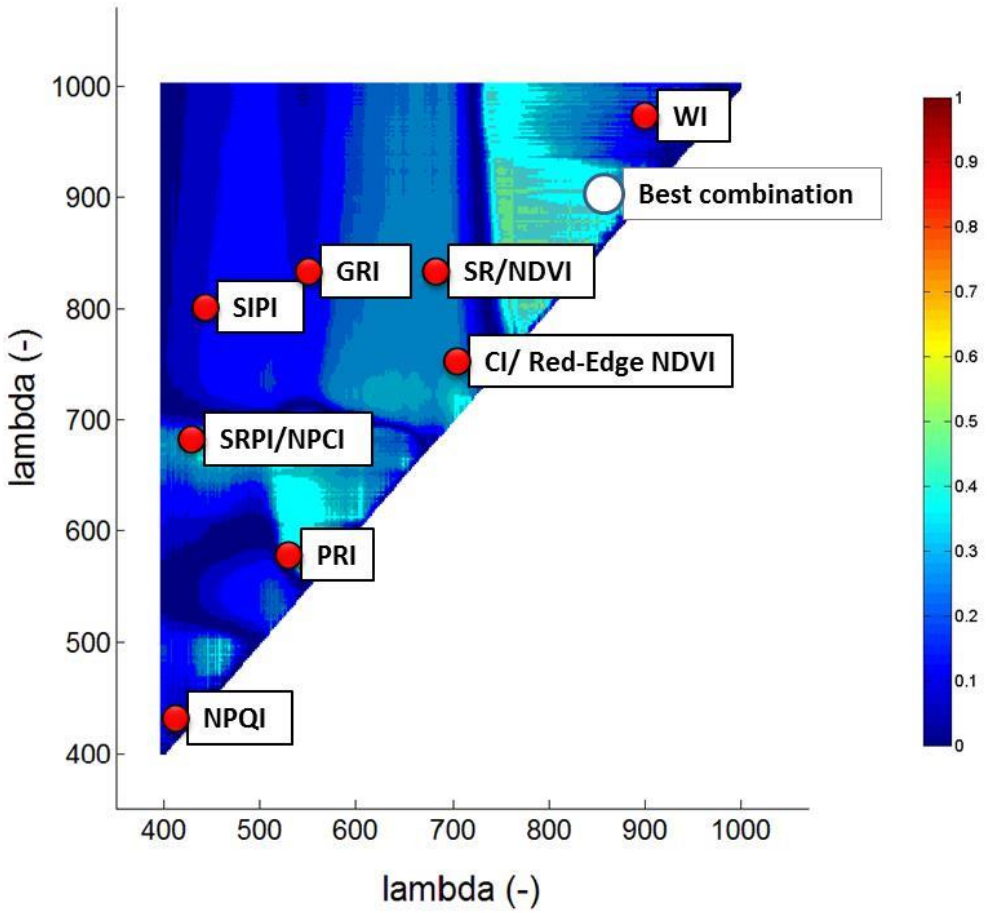

Figure 1. A selected example of a correlogram between NSD-type indices and midday average GPP for all sites pooled. The correlogram shows all R^2 values, the white dot indicates the two-band combination with the highest R^2 value and the red dots indicate the location of the reference VIs reported in Table 2 (SR: Simple ratio; GRI: Green Ratio Index; WI: Water Index; SRPI: Simple Ratio Pigment Index; NDVI: Normalized Difference Vegetation Index; NPQI: Normalized Phaeophytinization Index; NPCI: Normalized Pigment Chlorophyll Index; CI: Chlorophyll Index; Red Edge NDVI; SIPI: Structural Independent Pigment Index; PRI: Photochemical Reflectance Index).

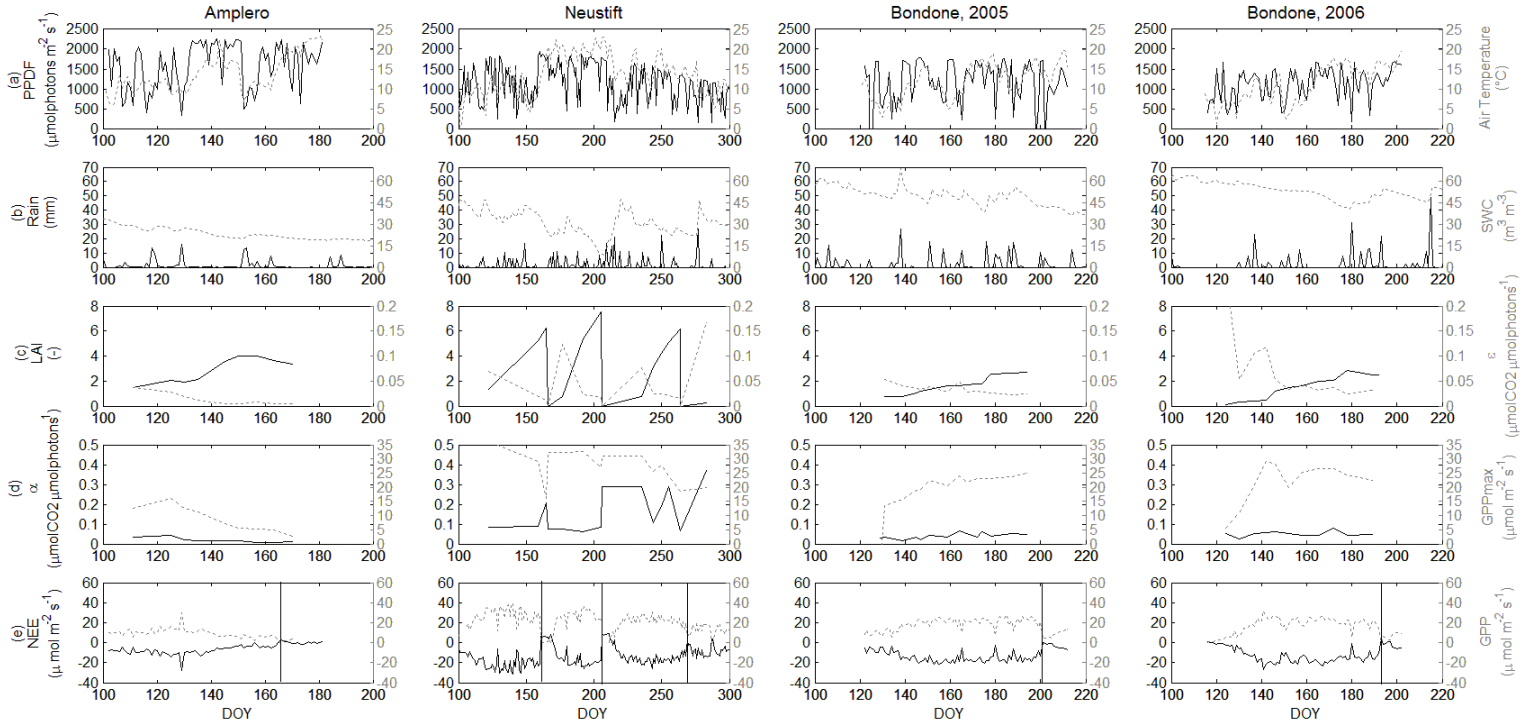

Figure 2. Seasonal variation of meteorological variables, LAI, CO_2 fluxes and ecophysiological parameters for the period of the hyperspectral measurements at the three investigated grasslands. (a) midday average photosynthetically active radiation (PAR; μmol m^{-2} s^{-1}; solid black line) and daily average air temperature (°C; dotted grey line); (b) daily precipitation (Rain; mm; solid black line) and daily average soil water content (SWC; m^3 m^{-3}; dotted grey line); (c) Leaf Area Index (LAI; m^2 m^{-2}; solid black line) and light use efficiency (ε; μmol photons μmol CO_2 $^{-1}$; dotted grey line); (d) apparent quantum yield (α; μmol CO_2 μmol photons $^{-1}$; solid black line) and gross primary production at saturating light (GPP_{max}; μmol m^{-2} s^{-1}; dotted grey line); (e) midday average net ecosystem CO_2 exchange (NEE; μmol m^{-2} s^{-1}; solid black line) and gross primary production (GPP; μmol m^{-2} s^{-1}; grey dotted line); vertical lines in the lowermost panels indicate the dates of mowing.

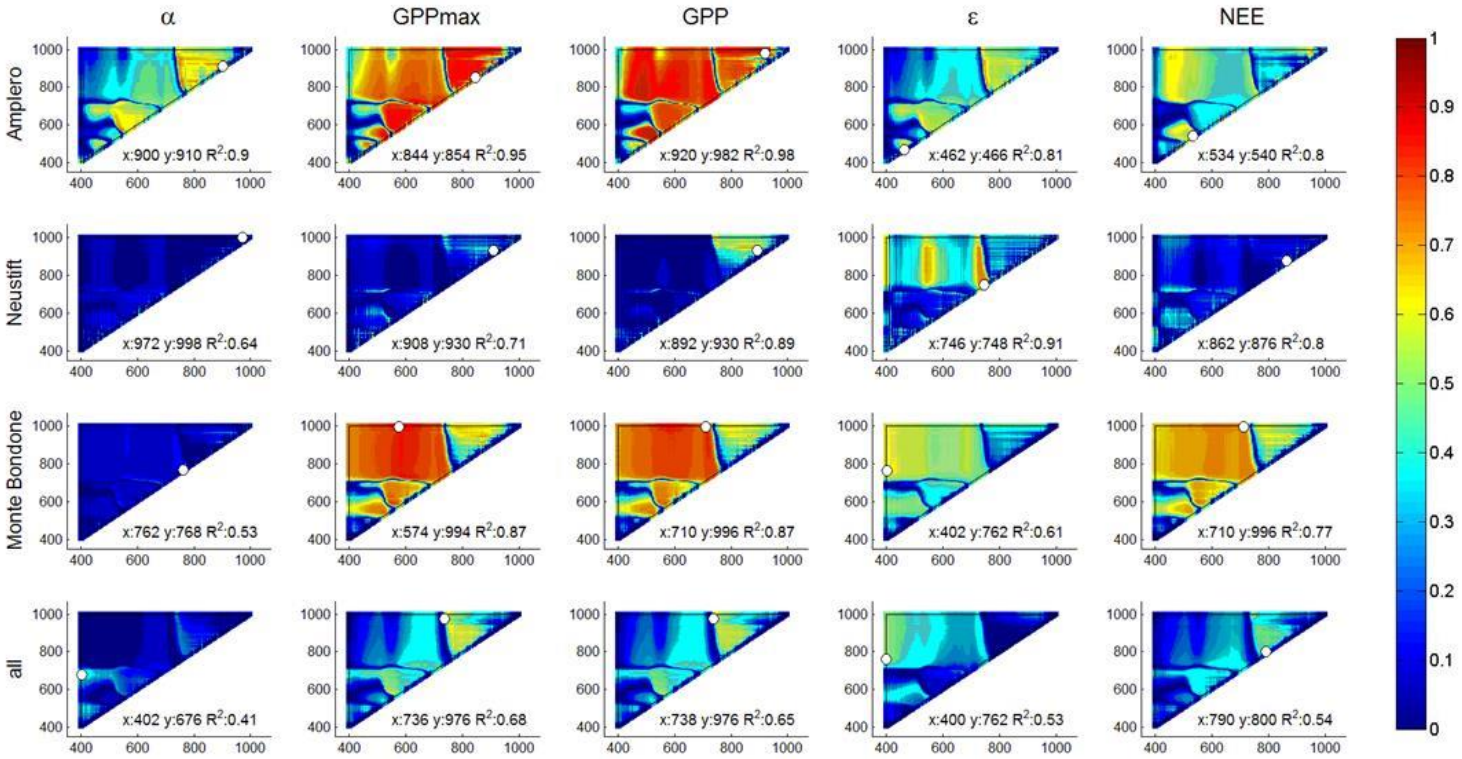

Figure 3. Correlograms of R^2 values for α, GPP_{max} and midday averaged GPP, ε and NEE and NSD-type indices for Amplero, Neustift, Monte Bondone (both study years pooled) and all sites pooled. The white dots indicate the position of paired band combinations corresponding to the maximum R^2.

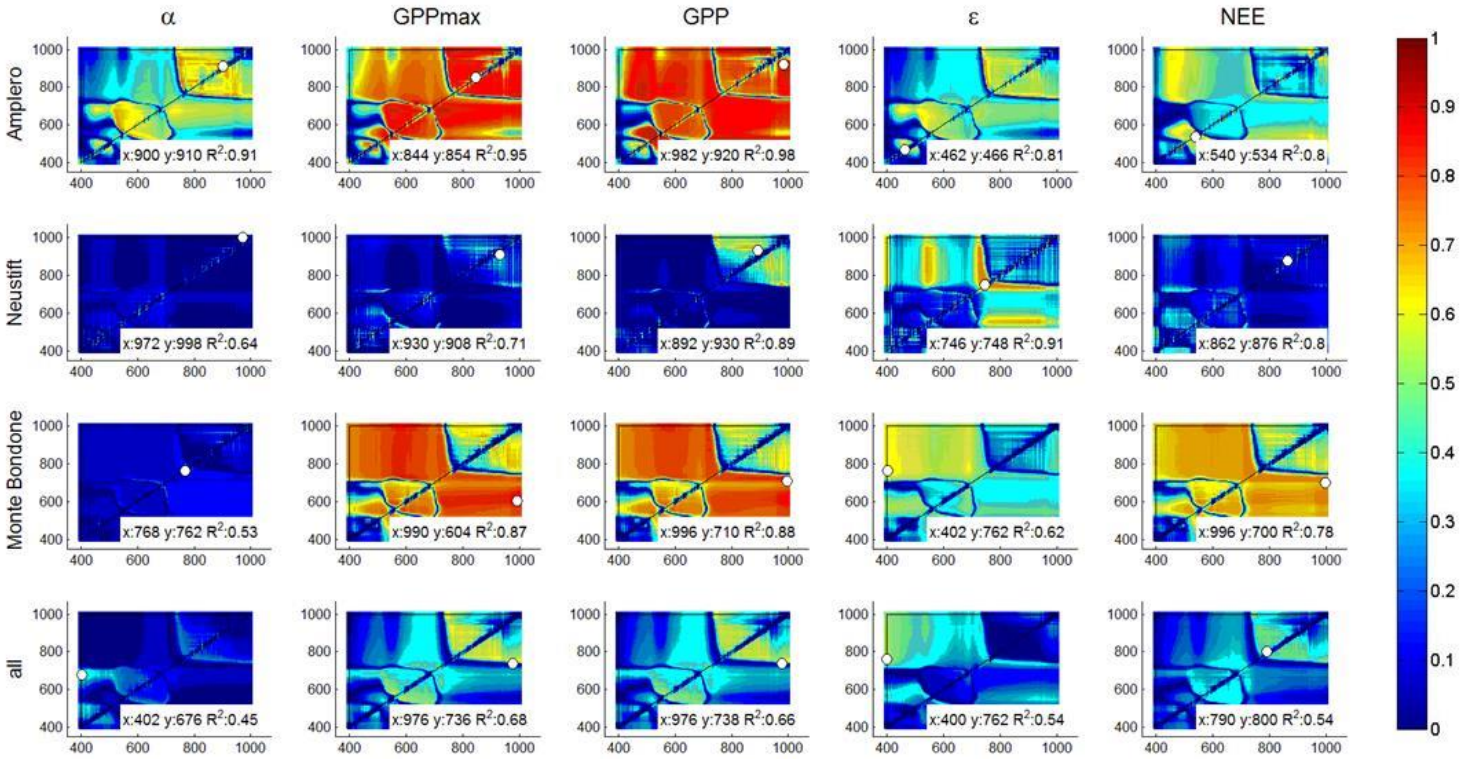

Figure 4. Correlograms of R^2 values for α, GPP_{max} and midday averaged GPP, ε and NEE and SR-type indices for Amplero, Neustift, Monte Bondone (both study years pooled) and all sites pooled. The white dots indicate the position of paired band combinations corresponding to the maximum R^2.

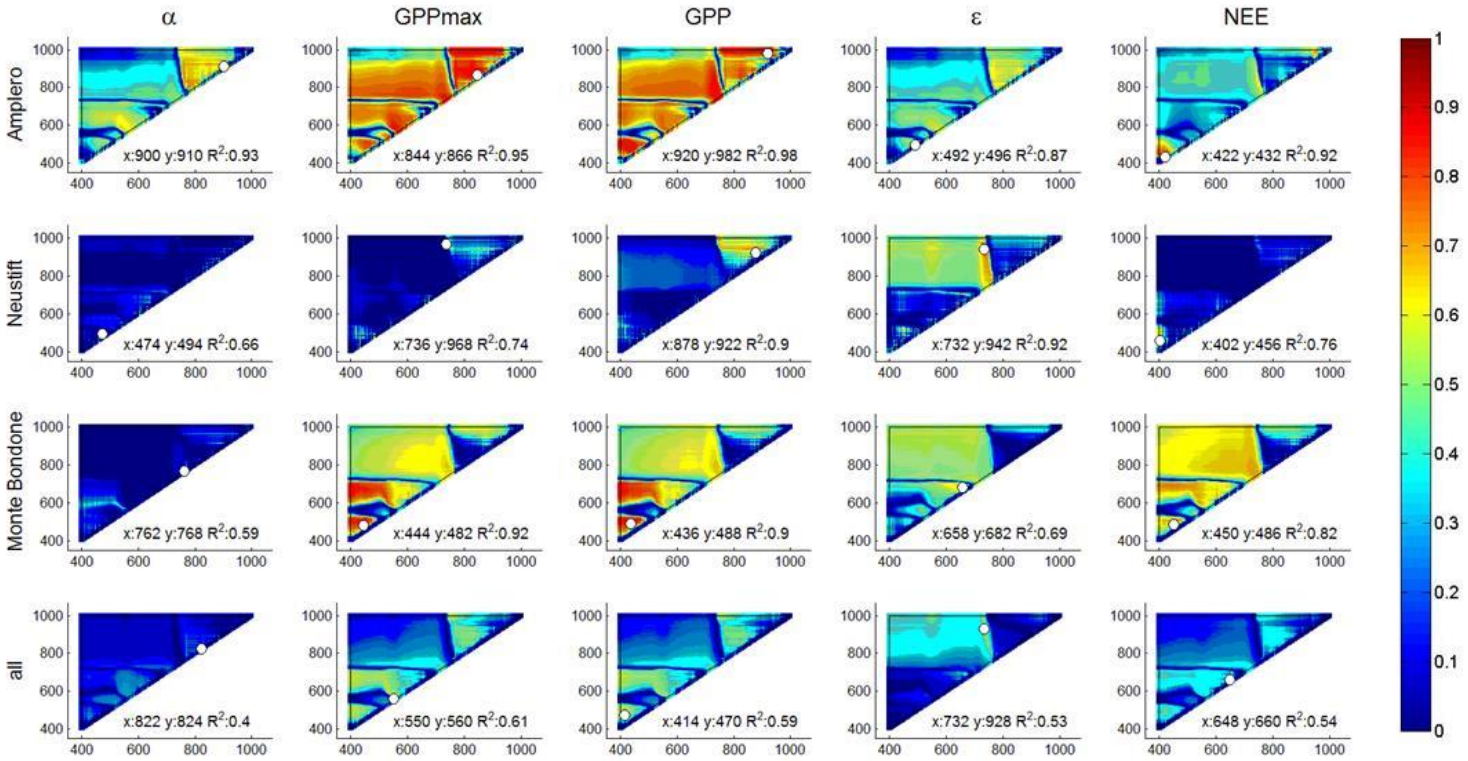

Figure 5. Correlograms of R^2 values for α, GPP_{max} and midday averaged GPP, ε and NEE and SD-type indices for Amplero, Neustift, Monte Bondone (both study years pooled) and all sites pooled. The white dots indicate the position of paired band combinations corresponding to the maximum R^2.

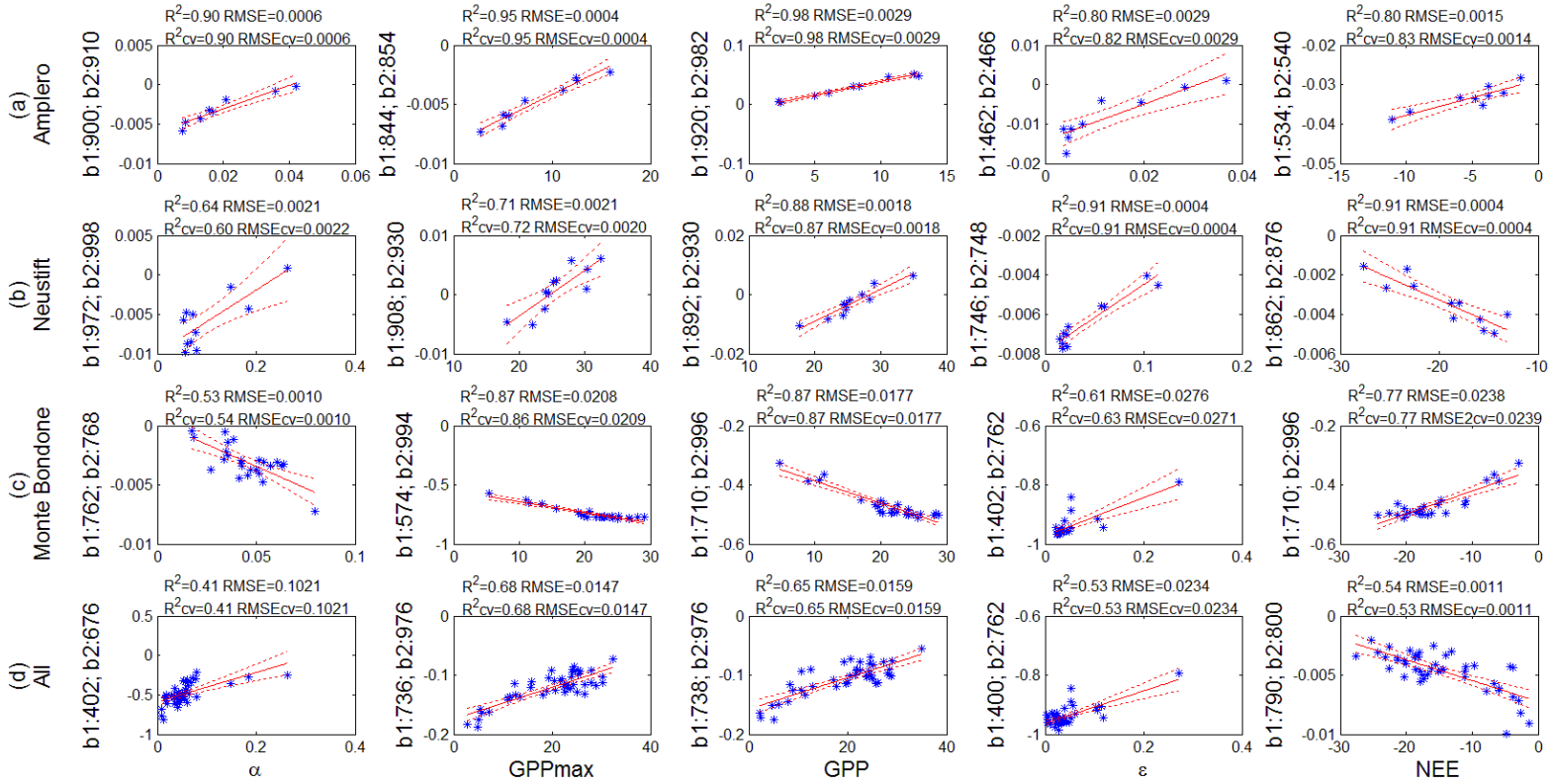

Figure 6. Results of linear correlation analysis for α, GPP_{max} and midday averaged GPP, ε and NEE and selected best NSD-type indices for (a) Amplero, (b) Neustift, (c) Monte Bondone (both study years pooled) and (d) all sites pooled. R^2—Coefficient of determination; RMSE—Root Mean Square Error; R^2cv—Cross-validated coefficient of determination; RMSEcv— Cross-validated root Mean Square Error. The solid red lines indicate the fitted models and the dotted red lines represent the 95% upper and lower confidence bounds.

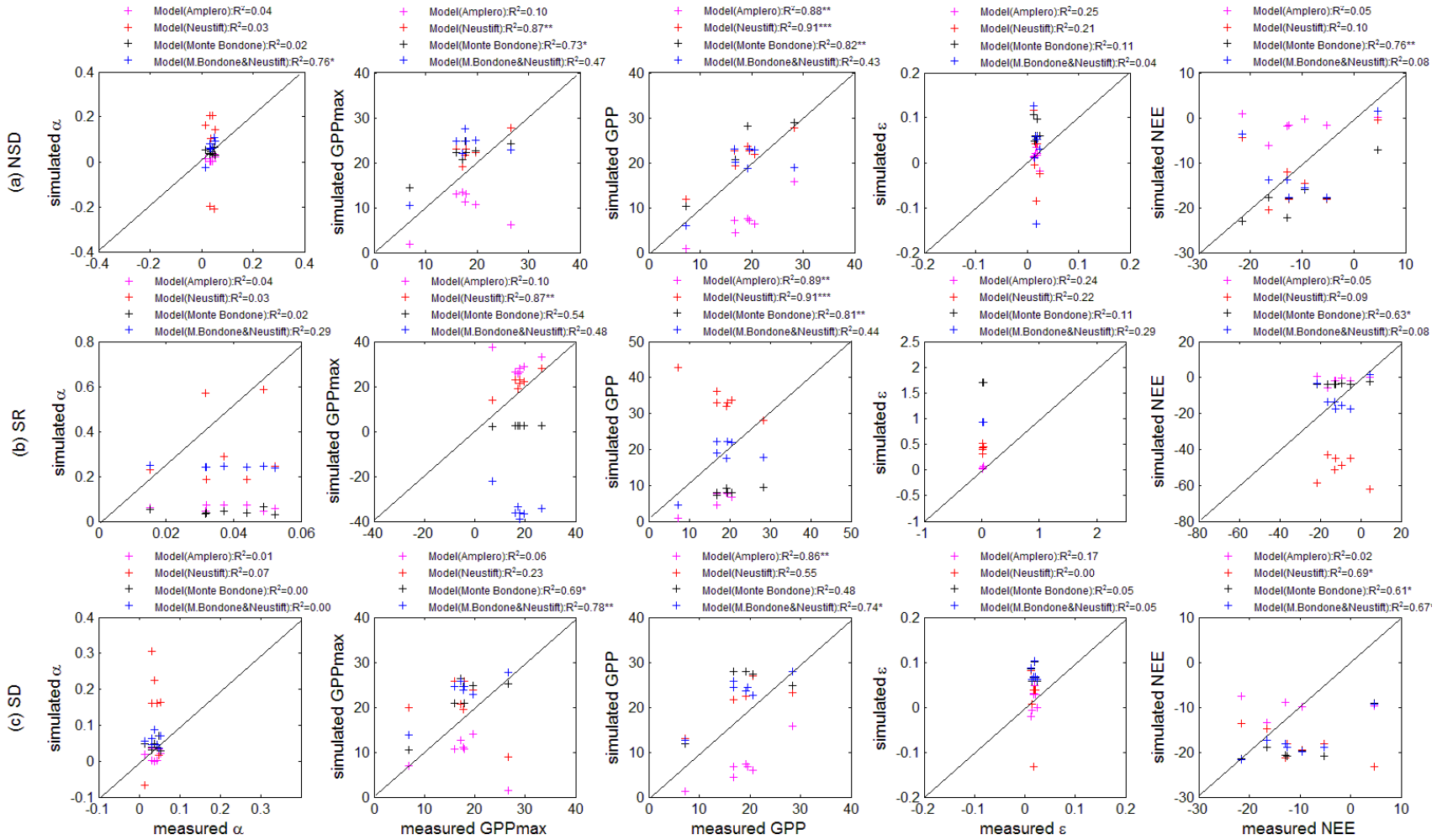

Figure 7. Results of validation of linear regression models between VIs ((a) NSD-type; (b) SR-type; (c) SD-type) and ecophysiological parameters: α, ε (midday average), GPP_{max} and midday average CO_2 fluxes (NEE and GPP). R^2 – coefficients of determination. Different colours represent results of the validation performed applying to the three new sites the model for Amplero (in magenta), Neustift (in red) and Monte Bondone (in blue) and a model parameterized grouping Monte Bondone & Neustift

(M.Bondone&Neustift; in black). Statistical significance is indicated as * ($p < 0.05$), ** ($p < 0.01$), and *** ($p < 0.001$). The black lines are 1:1 lines.

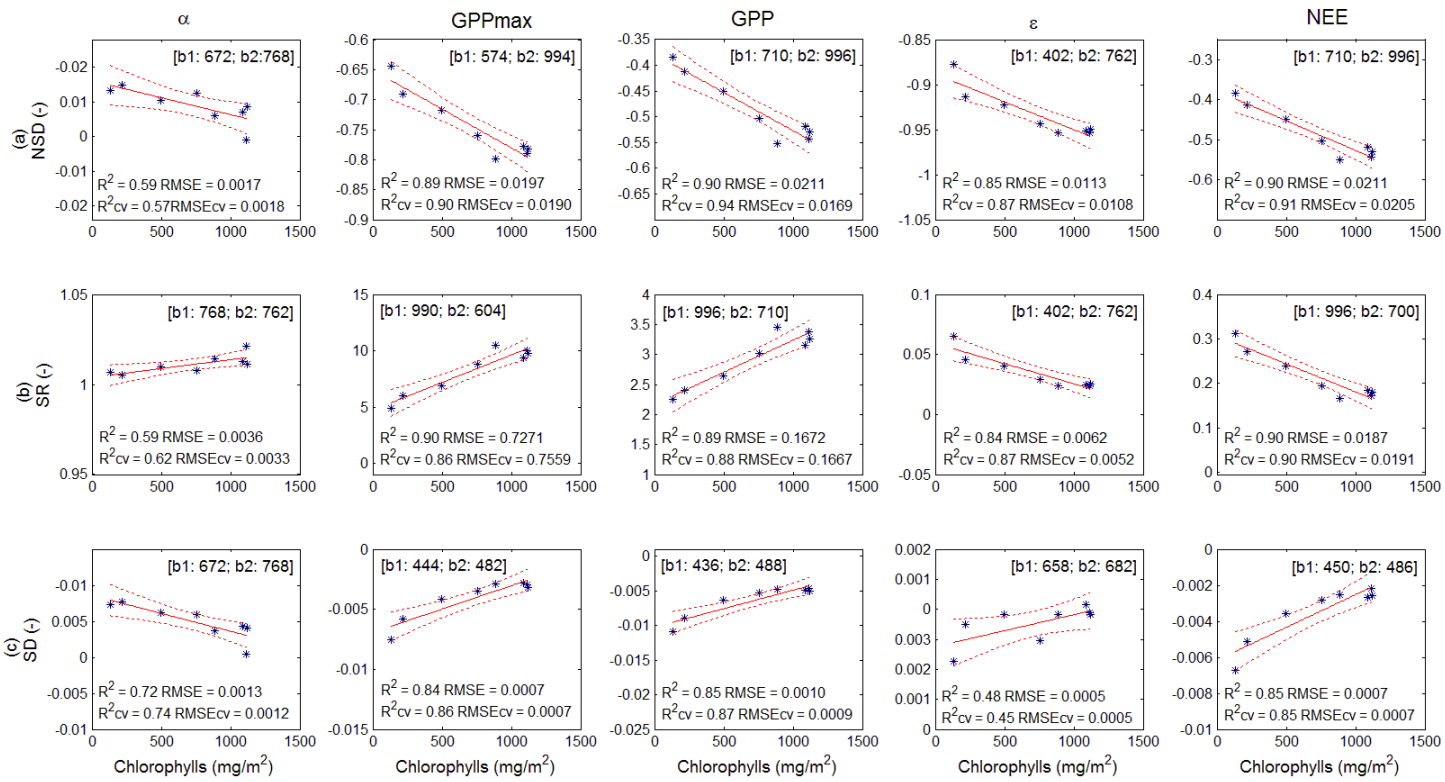

Figure 8. Correlation between selected (a) NSD-, (b) SR- and (c) SD-type indices for the α, GPP_{max}, midday GPP, midday ε and midday NEE (plots in the columns) and the total chlorophyll content for Monte Bondone in 2013. R^2— coefficient of correlation; RMSE—root mean square error; R^2cv— cross-validated coefficient of correlation; RMSEcv— cross-validated root mean square error.

The solid red lines indicate the fitted models and the dotted red lines represent the 95% upper and lower confidence bounds. The selected bands to compute NSD-, SR- and SD-type indices are reported in brackets.

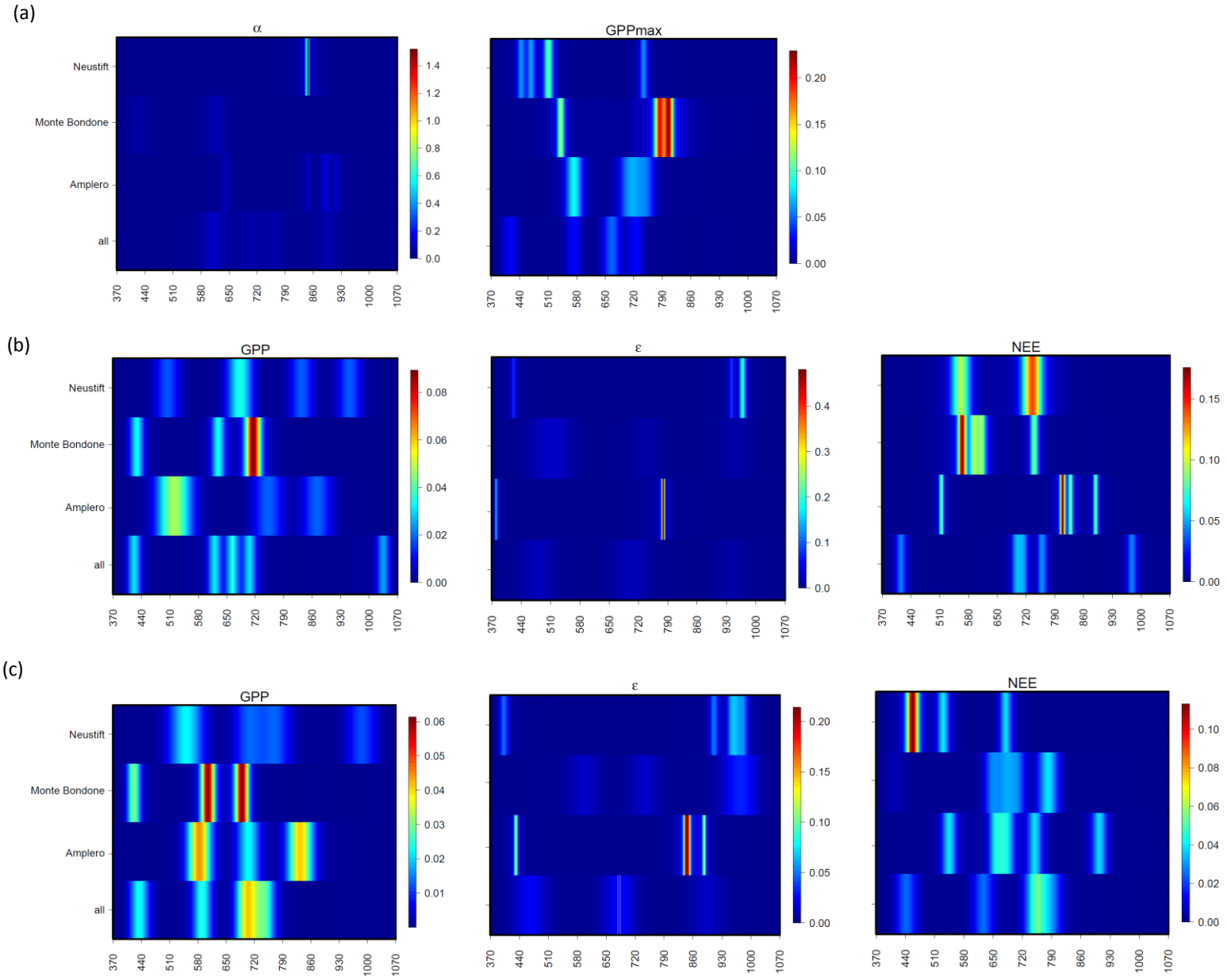
(a)
α
GPPmax
Neustift
Monte Bondone
Amplero
all
1.4
1.2
1.0
0.8
0.6
0.4
0.2
0.0
0.20
0.15
0.10
0.05
0.00
370
440
510
580
650
720
790
860
930
1000
1070
(b)
GPP
ε
NEE
0.08
0.06
0.04
0.02
0.00
0.4
0.3
0.2
0.1
0.0
0.15
0.10
0.05
0.00
(c)
GPP
ε
NEE
0.06
0.05
0.04
0.03
0.02
0.01
0.20
0.15
0.10
0.05
0.00
0.10
0.08
0.06
0.04
0.02
0.00

Figure 9. Results of the GA-rF method for band selection for Amplero, Neustift, Monte Bondone and all sites pooled for (a) α and GPP_{max}, (b) midday average ε, CO_2 fluxes (NEE and GPP); (b) daily average ε and CO_2 fluxes (NEE and GPP).

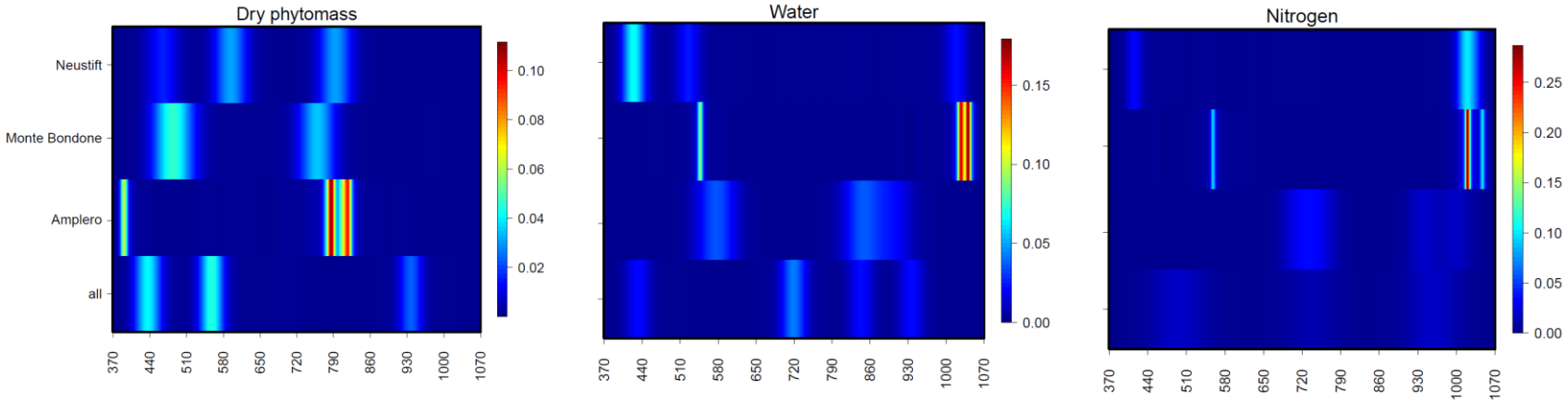

Figure 10. Results of the GA-rF method for band selection for Amplero, Neustift, Monte Bondone and all sites pooled for dry phytomass, water and nitrogen content.

Table 1. Description of the study sites and period.

Site characteristics	Amplero (IT-Amp)	Neustift (AT-Neu)	Monte Bondone (IT-MBo)
Latitude	41.9041	47.1162	46.0296
Longitude	13.6052	11.3204	11.0829
Elevation (m)	884	970	1550
Mean annual temperature (˚C)	10.0	6.5	5.5
Mean annual precipitation (mm)	1365	852	1189
Vegetation type	Seslerietum apenninae	Pastinaco–Arrhenatheretum	Nardetum Alpigenum
Study period[1]	111-170, 2006 (9)	122-303, 2006 (16)	129-201, 2005 (13) 124-192, 2006 (12)

[1] from-to DOY, year (number of hyperspectral measurement dates)

Table 2. Summary of the vegetation indices characteristics used in this study.

Index name and acronym	Formula	Use	Reference
Simple Spectral Ratio Indices			
Simple Ratio (SR or RVI)	$SR = R_{830}/R_{660}$	Greenness	Jordan (1969)
Green Ratio Index (GRI)	$GRI = R_{830}/R_{550}$	Greenness	Peñuelas and Filella (1998)
Water Index (WI)	$WI = R_{900}/R_{970}$	Water content, leaf water potential, canopy water content	Peñuelas et al. (1993)
Simple Ratio Pigment Index (SRPI)	$SRPI = (R_{430})/(R_{680})$		Peñuelas et al. (1995)
Chlorophyll Index (CI)	$CI = (R_{750}/R_{720}) - 1$	Chlorophyll content	Gitelson et al. (2005)
Normalized Spectral Difference Vegetation Indices			
Normalized Difference Vegetation Index (NDVI)	$NDVI = (R_{830}–R_{660})/(R_{830}+R_{660})$	Greenness	Rouse et al. (1973)
Normalized Phaeophytinization Index (NPQI)	$NPQI = (R_{415}–R_{435})/(R_{415}+R_{435})$	Carotenoid /Chlorophyll ratio	Barnes et al. (1992)
Normalized Pigment Chlorophyll Index (NPCI)	$NPCI = (R_{680} - R_{430})/ (R_{680} + R_{430})$	Chlorophyll ratio	Peñuelas et al. (1994)
Red-edge NDVI (Red-edge NDVI)	Red-edge $NDVI = (R_{750}–R_{720})/ (R_{750}+R_{720})$	Chlorophyll content	Gitelson and Merzlyak (1994)
Structural Independent Pigment Index (SIPI)	$SIPI=(R_{800}–R_{445})/(R_{800}+R_{445})$	Chlorophyll content	Peñuelas et al. (1995)

Table 3. Results of statistic of linear regression models between VIs and ecophysiological parameters: α, ε (midday average) and GPP_{max}. R^2—Coefficient of determination; and RMSE—Root Mean Square Error. Bold letters indicate the best fitting model.

	α								**ε**								**GPPmax**							
	Amplero		**Neustift**		**Monte Bondone**		**All**		**Amplero**		**Neustift**		**Monte Bondone**		**All**		**Amplero**		**Neustift**		**Monte Bondone**		**All**	
	R^2	**RMSE**	**R^2**	**RMSE**	**R^2**	**RMSE**	**R^2**	**RMSE**	**R^2**	**RMSE**	**R^2**	**RMSE**	**R^2**	**RMSE**	**R^2**	**RMSE**	**R^2**	**RMSE**	**R^2**	**RMSE**	**R^2**	**RMSE**	**R^2**	**RMSE**
VI	-	$\frac{\mu mol_{CO2}}{\mu mol_{phot}}$	-	$\frac{\mu mol_{CO2}}{\mu mol_{phot}}$	-	$\frac{\mu mol_{CO2}}{\mu mol_{phot}}$	-	$\frac{\mu mol_{CO2}}{\mu mol_{phot}}$	-	$\frac{\mu mol_{CO2}}{\mu mol_{phot}}$	-	$\frac{\mu mol_{CO2}}{\mu mol_{phot}}$	-	$\frac{\mu mol_{CO2}}{\mu mol_{phot}}$	-	$\frac{\mu mol_{CO2}}{\mu mol_{phot}}$	-	$\frac{\mu mol_{CO2}}{\mu mol_{phot}}$	-	$\frac{\mu mol_{CO2}}{\mu mol_{phot}}$	-	$\frac{\mu mol_{CO2}}{\mu mol_{phot}}$	-	$\frac{\mu mol_{CO2}}{\mu mol_{phot}}$
SR	0.57	0.01	0.04	0.07	**0.13**	0.01	0.06	0.04	0.50	0.01	0.33	0.03	0.35	0.04	0.18	0.04	**0.89**	1.58	0.01	4.31	0.78	2.76	0.28	6.71
GRI	0.29	0.01	0.00	0.07	0.13	0.01	0.00	0.05	0.26	0.01	**0.67**	0.02	0.44	0.04	**0.47**	0.03	0.69	2.66	0.00	4.35	0.81	2.53	0.09	7.51
WI	0.50	0.01	0.01	0.07	0.08	0.01	0.03	0.04	0.41	0.01	0.22	0.03	0.36	0.04	0.25	0.04	0.86	1.82	0.16	3.99	0.54	3.95	0.24	6.87
NDVI	0.44	0.01	0.04	0.07	0.06	0.01	0.06	0.04	0.40	0.01	0.30	0.03	0.53	0.04	0.43	0.03	0.79	2.21	0.03	4.28	**0.82**	2.50	0.37	6.27
SIPI	0.37	0.01	**0.07**	0.07	0.02	0.01	0.18	0.04	0.35	0.01	0.29	0.03	**0.64**	0.03	0.44	0.03	0.66	2.80	0.06	4.21	0.74	2.96	**0.47**	5.74
CI	0.49	0.01	0.00	0.07	0.09	0.01	0.01	0.05	0.41	0.01	0.65	0.02	0.43	0.04	0.34	0.04	0.81	2.08	0.01	4.34	0.80	2.62	0.16	7.24
PRI	**0.71**	0.01	0.02	0.07	0.02	0.01	0.14	0.04	0.50	0.01	0.19	0.03	0.28	0.05	0.40	0.04	0.41	3.68	**0.26**	3.75	0.11	5.50	0.14	7.33
EVI	0.47	0.01	0.03	0.07	0.03	0.01	0.14	0.04	0.46	0.01	0.43	0.03	0.53	0.04	0.38	0.04	0.78	2.25	0.01	4.33	0.70	3.21	0.32	6.50
NPQI	0.06	0.01	0.06	0.07	0.05	0.01	0.31	0.04	0.04	0.01	0.30	0.03	0.17	0.05	0.11	0.04	0.00	4.78	0.07	4.20	0.21	5.17	0.14	7.31
NPCI	0.50	0.01	0.07	0.07	0.03	0.01	**0.37**	0.04	0.51	0.01	0.17	0.03	0.00	0.05	0.00	0.05	0.53	3.28	0.17	3.97	0.17	5.33	0.32	6.52
SRPI	0.51	0.01	0.06	0.07	0.03	0.01	0.36	0.04	**0.56**	0.01	0.15	0.04	0.00	0.05	0.00	0.05	0.50	3.38	0.17	3.97	0.17	5.31	0.28	6.69
RedEdgeNDVI	0.48	0.01	0.00	0.07	0.07	0.01	0.01	0.05	0.40	0.01	0.65	0.02	0.47	0.04	0.40	0.04	0.79	2.16	0.00	4.34	0.80	2.58	0.19	7.09

Table 4. Results of statistic of linear regression models between VIs and midday average CO_2 fluxes: NEE and GPP. R^2—Coefficient of determination; and RMSE—Root Mean Square Error. Bold letters indicate the best fitting model.

	GPP								NEE							
	Amplero		Neustift		Monte Bondone		All		Amplero		Neustift		Monte Bondone		All	
	R^2	RMSE	R^2	RMSE	R^2	RMSE	R^2	RMSE	R^2	RMSE	R^2	RMSE	R^2	RMSE	R^2	RMSE
	-	$\frac{\mu mol_{CO2}}{m^2 s}$	-	$\frac{\mu mol_{CO2}}{m^2 s}$	-	$\frac{\mu mol_{CO2}}{m^2 s}$	-	$\frac{\mu mol_{CO2}}{m^2 s}$	-	$\frac{\mu mol_{CO2}}{m^2 s}$	-	$\frac{\mu mol_{CO2}}{m^2 s}$	-	$\frac{\mu mol_{CO2}}{m^2 s}$	-	$\frac{\mu mol_{CO2}}{m^2 s}$
SR	0.86	1.59	0.08	4.56	0.75	3.12	0.27	7.09	0.36	2.76	0.08	4.77	0.68	3.19	0.18	6.35
GRI	0.85	1.67	0.01	4.44	0.80	2.78	0.10	7.85	**0.54**	2.32	0.01	4.96	0.68	3.21	0.08	6.73
WI	**0.92**	1.23	0.05	3.25	0.50	4.41	0.24	7.20	0.44	2.57	0.05	4.87	0.43	4.28	0.17	6.42
NDVI	0.82	1.79	**0.14**	4.58	0.80	2.82	0.36	6.60	0.42	2.63	**0.14**	4.63	0.72	3.01	0.29	5.94
SIPI	0.65	2.50	0.08	4.57	0.72	3.32	**0.46**	6.08	0.33	2.82	0.08	4.79	0.65	3.34	**0.39**	5.51
CI	0.88	1.44	0.00	4.31	0.81	2.69	0.17	7.56	0.43	2.59	0.00	4.98	**0.75**	2.82	0.12	6.59
PRI	0.25	3.69	0.05	4.34	0.14	5.79	0.10	7.84	0.00	3.44	0.05	4.87	0.15	5.20	0.05	6.84
EVI	0.75	2.11	0.01	4.31	0.68	3.51	0.33	6.79	0.36	2.74	0.01	4.97	0.71	3.03	0.26	6.05
NPQI	0.04	4.17	0.08	4.27	0.14	5.78	0.16	7.57	0.24	2.99	0.08	4.78	0.19	5.08	0.12	6.60
NPCI	0.40	3.29	0.01	4.45	0.14	5.76	0.30	6.92	0.11	3.25	0.01	4.95	0.21	5.03	0.25	6.09
SRPI	0.35	3.42	0.01	4.44	0.15	5.74	0.27	7.08	0.08	3.30	0.01	4.95	0.22	5.01	0.22	6.19
RedEdgeNDVI	0.87	1.51	0.00	4.35	**0.81**	2.68	0.20	7.40	0.43	2.60	0.00	4.98	0.75	2.84	0.15	6.47

Table 5. Results of the correlation (R^2—Coefficient of determination) between the best NDS, SR and SD-type indices selected for the α, GPP_{max}, midday GPP, midday ε and midday NEE and dry phytomass, nitrogen and water content for Amplero, Neustift, Monte Bondone and all sites pooled. The selected bands to compute NSD-, SR- and SD-type indices are reported in brackets. Statistical significance is indicated as * ($p < 0.05$), ** ($p < 0.01$), and *** ($p < 0.001$).

Index	Site	Parameter	α R^2 (-)	GPPmax R^2 (-)	GPP R^2 (-)	ε R^2 (-)	NEE R^2 (-)
NSD-type	Amplero	Dry phytomass (g m^{-2})	0.66**	0.72**	0.58*	0.76**	0.36
	Amplero	Nitrogen content (%)	0.30	0.32	0.19	0.49*	0.15
	Amplero	Water content (%)	0.28	0.53*	0.56*	0.44	0.55*
	Neustift	Dry phytomass (g m^{-2})	0.00	0.26	0.35	0.44*	0.02
	Neustift	Nitrogen content (%)	0.16	0.15	0.21	0.77**	0.03
	Neustift	Water content (%)	0.00	0.00	0.03	0.59*	0.10
	Monte Bondone	Dry phytomass (g m^{-2})	0.02	0.59***	0.49***	0.55***	0.49***
	Monte Bondone	Nitrogen content (%)	0.08	0.52***	0.38**	0.48***	0.38**
	Monte Bondone	Water content (%)	0.09	0.48***	0.35**	0.42***	0.35**
	All	Dry phytomass (g m^{-2})	0.05	0.02	0.02	0. 05	0.00
	All	Nitrogen content (%)	0.26***	0.04	0.02	0.41***	0.09
	All	Water content (%)	0.00	0.01	0.01	0.10*	0.00
SR-type	Amplero	Dry phytomass (g m^{-2})	0.66**	0.72**	0.58*	0.76*	0.36
	Amplero	Nitrogen content (%)	0.30	0.32	0.20	0.49*	0.15
	Amplero	Water content (%)	0.28	0.53*	0.56*	0.44	0.55*
	Neustift	Dry phytomass (g m^{-2})	0.00	0.26	0.35	0.44*	0.02
	Neustift	Nitrogen content (%)	0.16	0.15	0.21	0.77**	0.03
	Neustift	Water content (%)	0.01	0.00	0.03	0.59*	0.10
	Monte Bondone	Dry phytomass (g m^{-2})	0.02	0.50***	0.50***	0.55***	0.45*
	Monte Bondone	Nitrogen content (%)	0.08	0.48***	0.38**	0.48***	0.35
	Monte Bondone	Water content (%)	0.09	0.44***	0.34**	0.41***	0.30*
	All	Dry phytomass (g m^{-2})	0.08	0.01	0.01	0.05	0.00
	All	Nitrogen content (%)	0.26***	0.03	0.02	0.40***	0.09
	All	Water content (%)	0.00	0.01	0.01	0.11*	0.00
SD-type	Amplero	Dry phytomass (g m^{-2})	0.64***	0.81**	0.59*	0.58*	0.25
	Amplero	Nitrogen content (%)	0.22	0.30	0.22	0.30	0.03

Amplero	Water content (%)	0.16	0.45*	0.59*	0.19	0.49*
Neustift	Dry phytomass (g m^{-2})	0.21	0.04	0.37	0.20	0.00
Neustift	Nitrogen content (%)	0.11	0.01	0.12	0.81**	0.08
Neustift	Water content (%)	0.02	0.26	0.00	0.64*	0.52*
Monte Bondone	Dry phytomass (g m^{-2})	0.15	0.42***	0.36**	0.45***	0.36**
Monte Bondone	Nitrogen content (%)	0.28***	0.34**	0.34**	0.38**	0.35**
Monte Bondone	Water content (%)	0.27***	0.34**	0.34	0.31**	0.30**
All	Dry phytomass (g m^{-2})	0.20***	0.01	0.00	0.30***	0.01
All	Nitrogen content (%)	0.01	0.01	0.02	0.02	0.11*
All	Water content (%)	0.01	0.03	0.04	0.28***	0.06

Figures

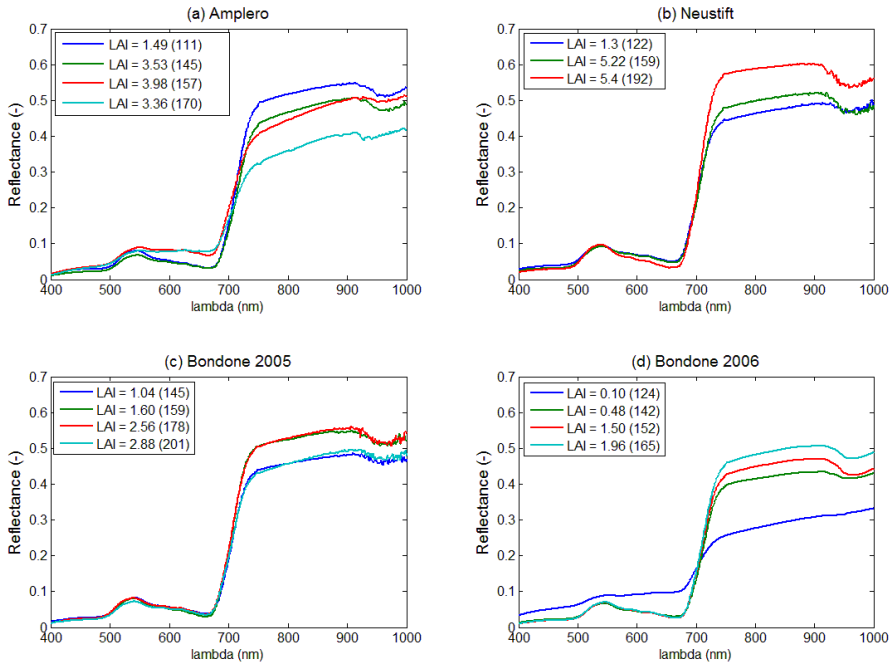

Figure S1. Selected grassland spectral signatures during the growing seasons. The figure legends indicates the corresponding leaf area index (LAI; m^2 m^{-2}) and the day of year (in parenthesis).

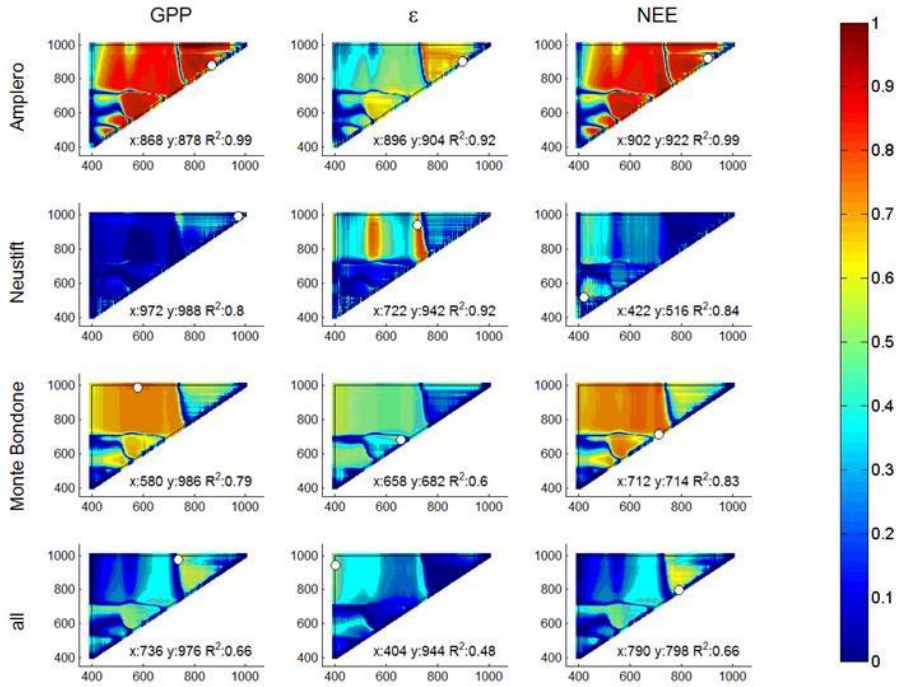

Figure S2. Correlograms of R^2 values for daily averaged GPP, ε and NEE and NSD-type indices for Amplero, Neustift, Monte Bondone (both study years pooled) and all sites pooled. The white dots indicate the position of paired band combinations corresponding to the maximum R^2.

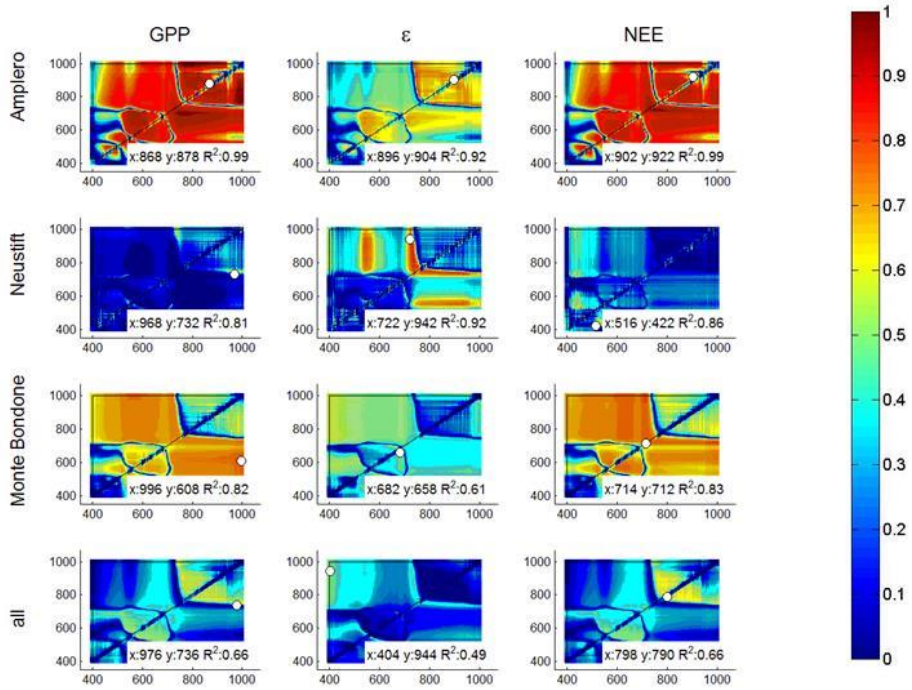

Figure S3. Correlograms of R^2 values for daily averaged GPP, ε and NEE and SR-type indices for Amplero, Neustift, Monte Bondone (both study years pooled) and all sites pooled. The white dots indicate the position of paired band combinations corresponding to the maximum R^2.

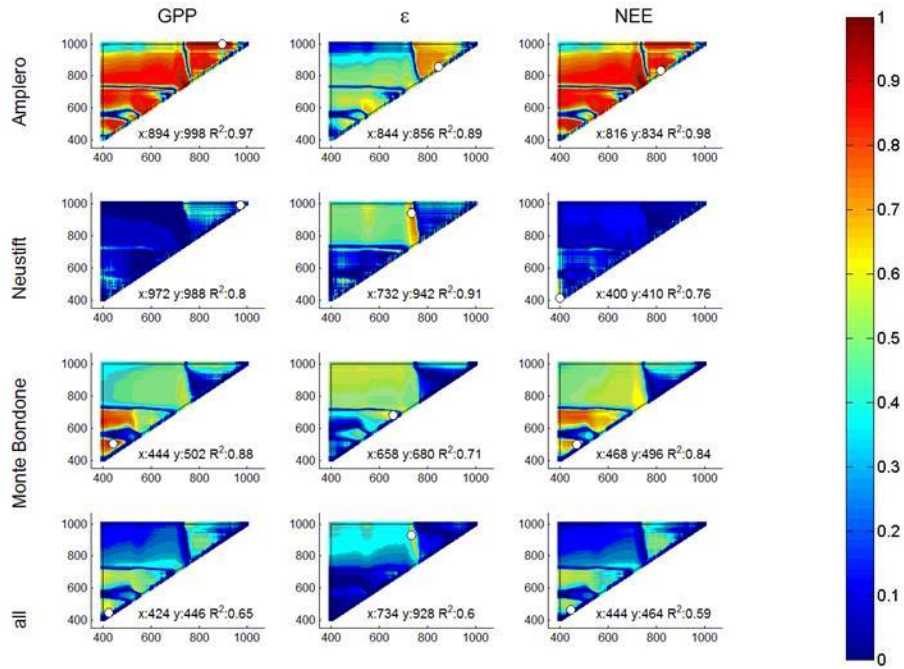

Figure S4. Correlograms of R^2 values for daily averaged GPP, ε and NEE and SD-type indices for Amplero, Neustift, Monte Bondone (both study years pooled) and all sites pooled. The white dots indicate the position of paired band combinations corresponding to the maximum R^2.

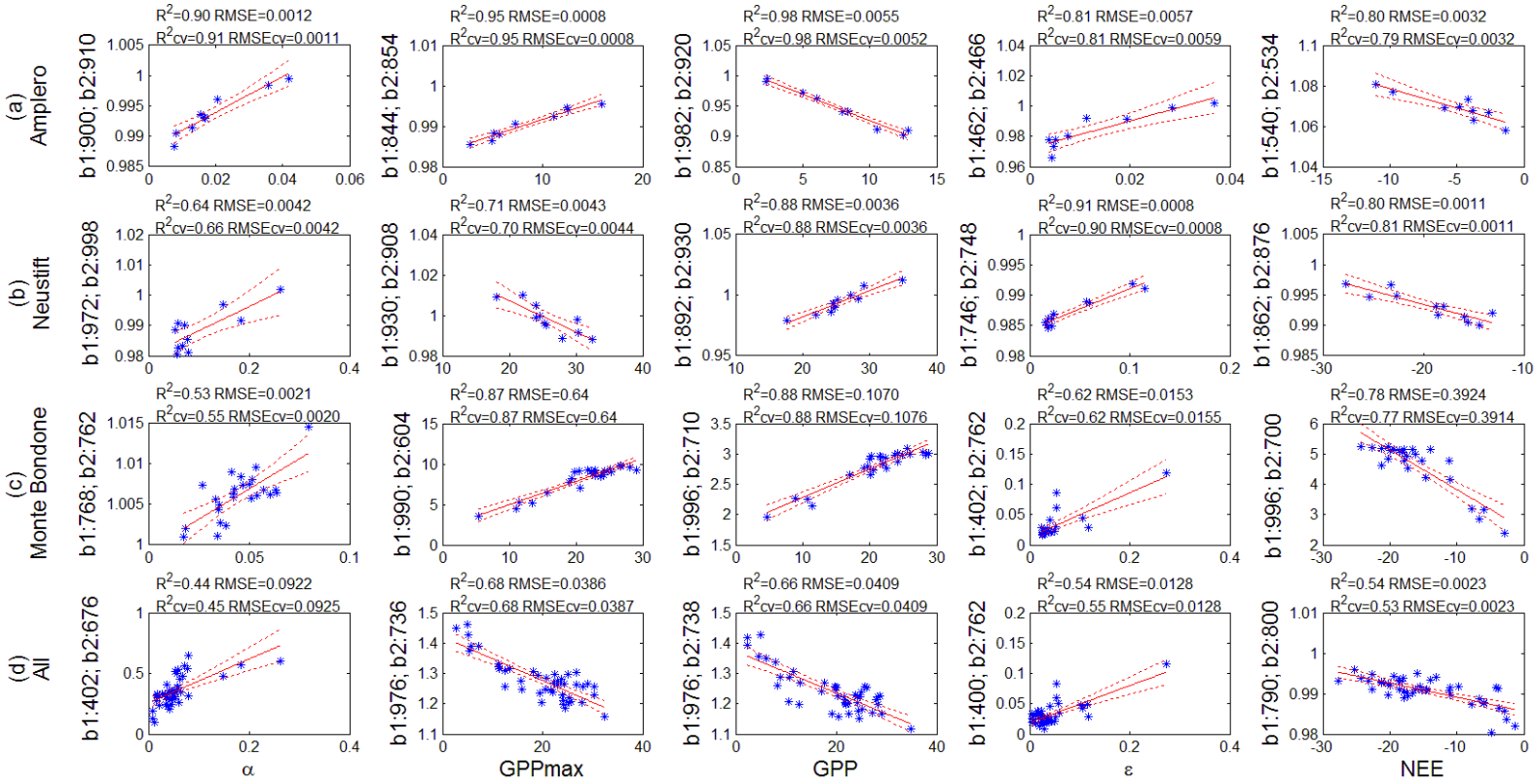

Figure S5. Results of linear correlation analysis for α, GPP_{max} and midday averaged GPP, ε and NEE and selected best SR-type indices for (a) Amplero, (b) Neustift, (c) Monte Bondone (both study years pooled) and (d) all sites pooled. R^2—Coefficient of determination; RMSE—Root Mean Square Error; R^2cv—Cross-validated coefficient of determination; RMSEcv— Cross-validated root Mean Square Error. The solid red lines indicate the fitted models and the dotted red lines represent the 95% upper and lower confidence bounds.

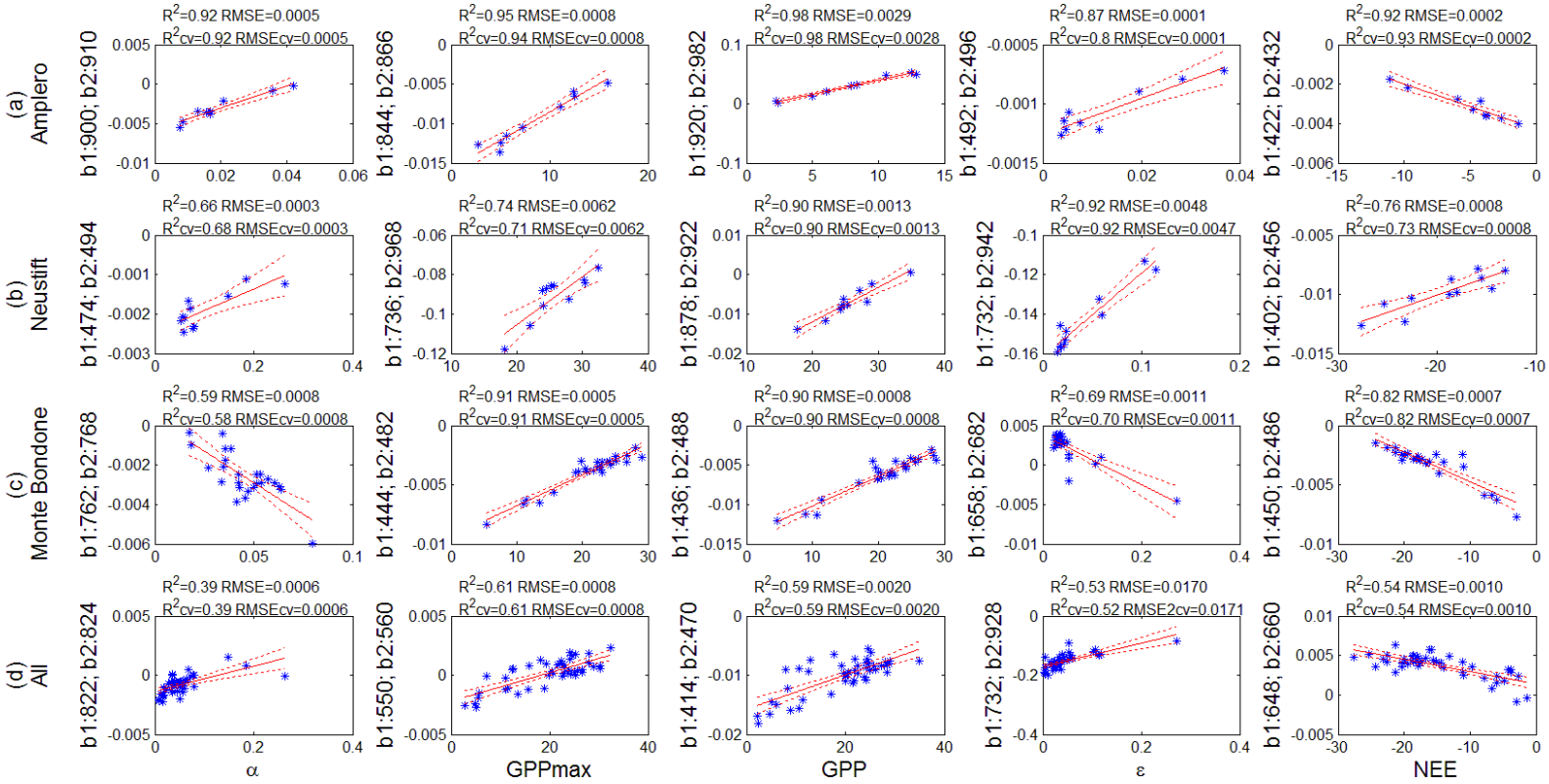

Figure S6. Results of linear correlation analysis for α, GPP_{max} and midday averaged GPP, ε and NEE and selected SD-type indices for (a) Amplero, (b) Neustift, (c) Monte Bondone (both study years pooled) and (d) all sites pooled. R^2—Coefficient of determination; RMSE—Root Mean Square Error; R^2cv—Cross-validated coefficient of determination; RMSEcv— Cross-validated root Mean Square Error. The solid red lines indicate the fitted models and the dotted red lines represent the 95% upper and lower confidence bounds.

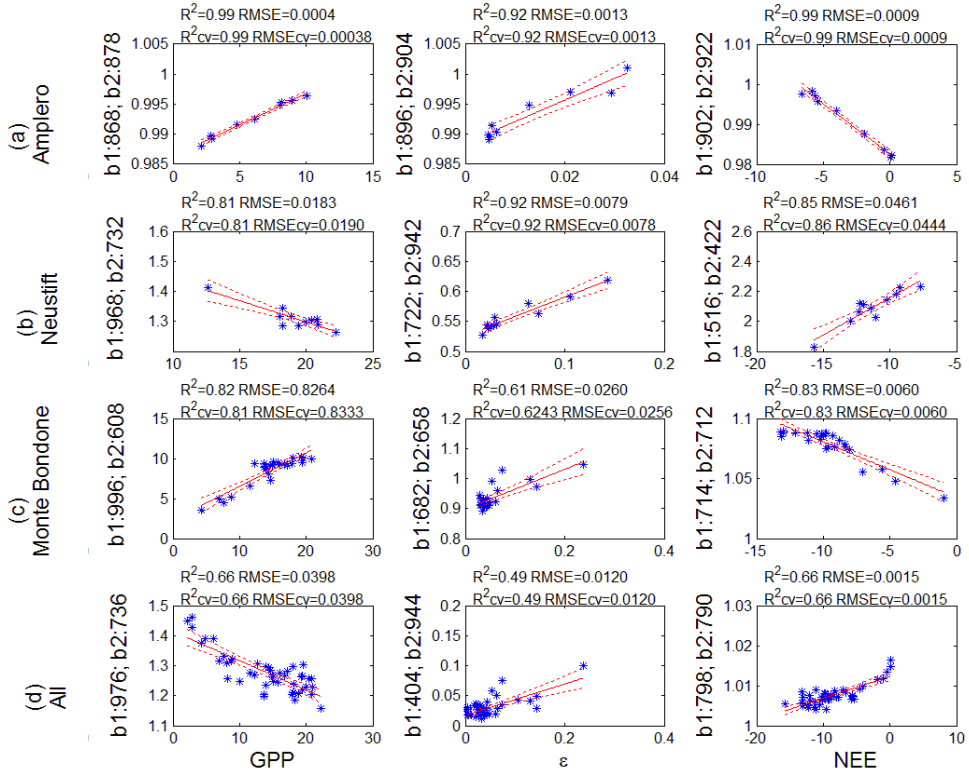

Figure S7. Results of linear correlation analysis for daily averaged GPP, ε and NEE and selected NSD-type indices for (a) Amplero, (b) Neustift, (c) Monte Bondone (both study years pooled) and (d) all sites pooled. R^2—Coefficient of determination; RMSE—Root Mean Square Error; R^2cv—Cross-validated coefficient of determination; RMSEcv— Cross-validated root Mean Square Error. The solid red lines indicate the fitted models and the dotted red lines represent the 95% upper and lower confidence bounds.

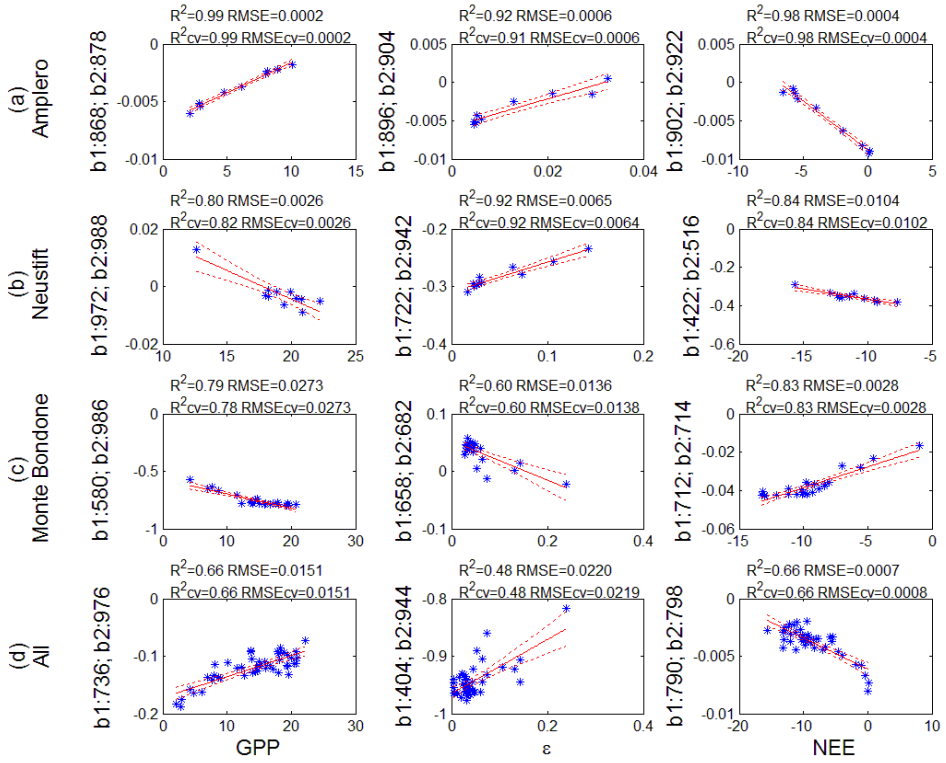

Figure S8. Results of linear correlation analysis for daily averaged GPP, ε and NEE and selected SR-type indices for (a) Amplero, (b) Neustift, (c) Monte Bondone (both study years pooled) and (d) all sites pooled. R^2—Coefficient of determination; RMSE—Root Mean Square Error; R^2cv—Cross-validated coefficient of determination; RMSEcv— Cross-validated root Mean Square Error. The solid red lines indicate the fitted models and the dotted red lines represent the 95% upper and lower confidence bounds.

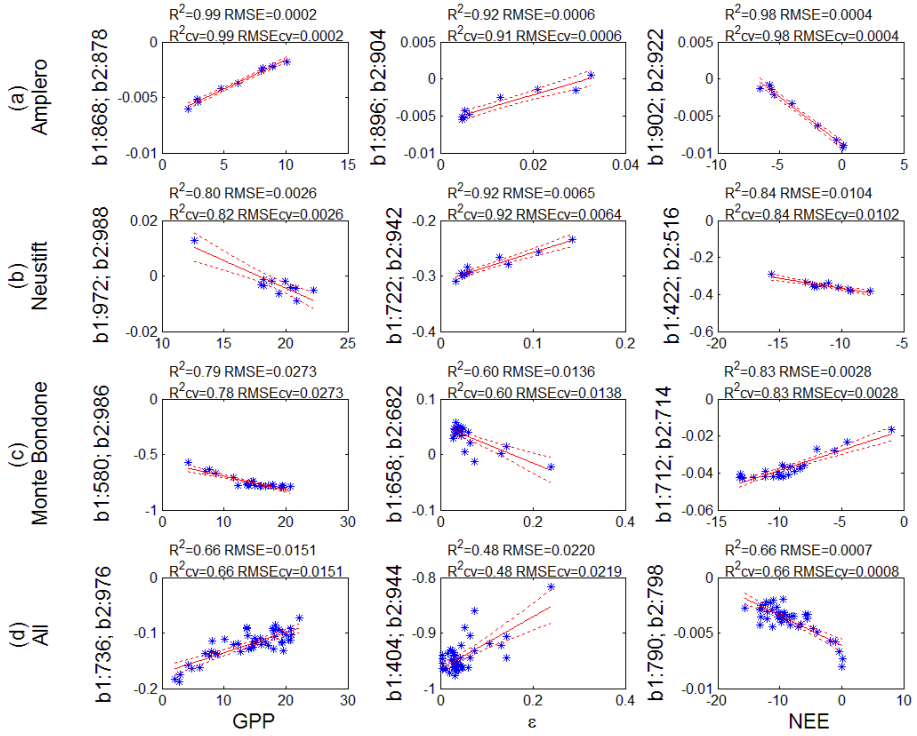

Figure S9. Results of linear correlation analysis for daily averaged GPP, ε and NEE and selected SD-type indices for (a) Amplero, (b) Neustift, (c) Monte Bondone (both study years pooled) and (d) all sites pooled. R^2—Coefficient of determination; RMSE—Root Mean Square Error; R^2cv—Cross-validated coefficient of determination; RMSEcv— Cross-validated root Mean Square Error. The solid red lines indicate the fitted models and the dotted red lines represent the 95% upper and lower confidence bounds.

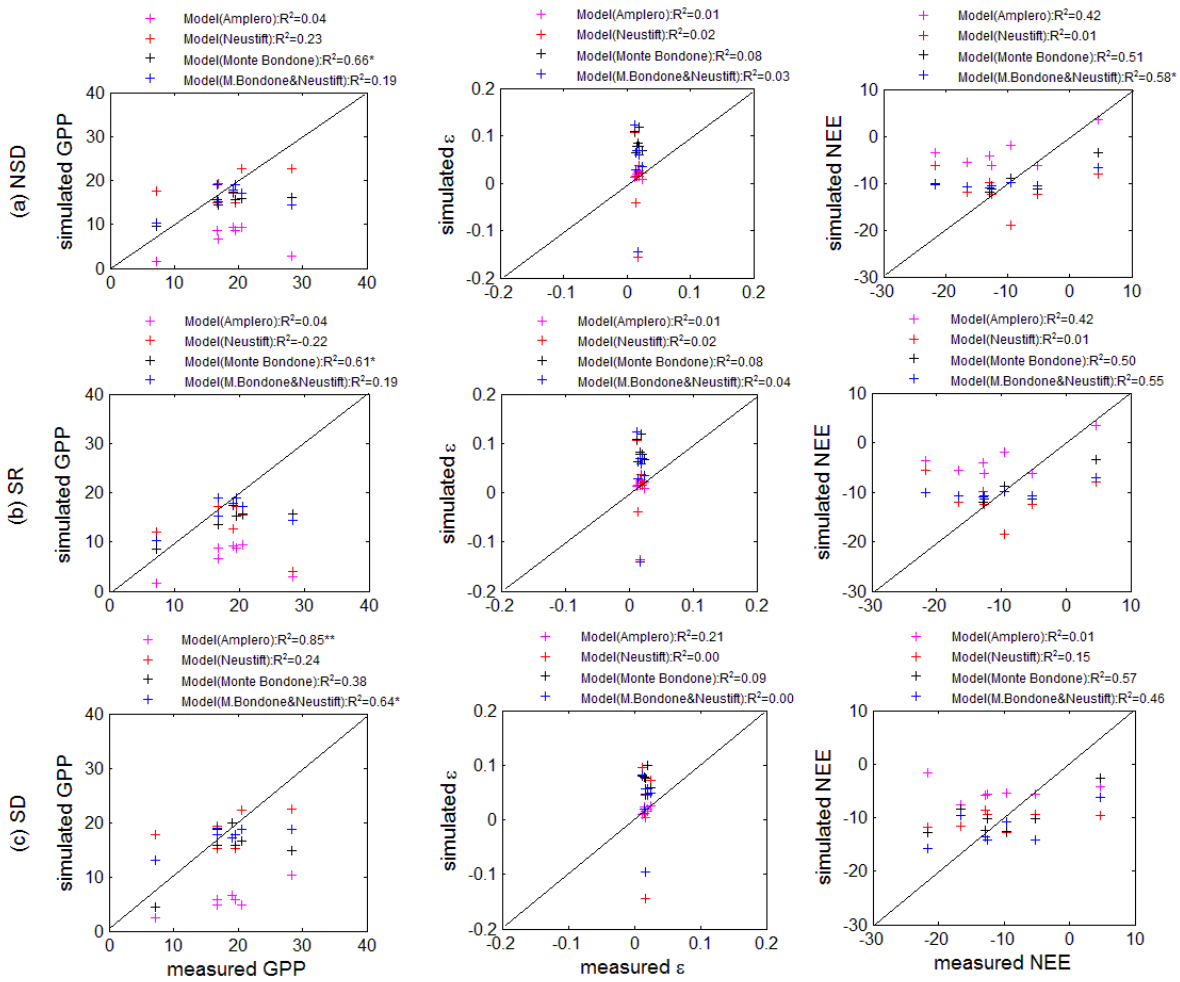

Figure S10. Results of validation of linear regression models between VIs ((a) NSD-type; (b) SR-type; (c) SD-type) and daily average ε and CO_2 fluxes (NEE and GPP). R^2 – coefficients of determination. Different colours represent results of the validation performed applying to the three new sites the model for Amplero (in magenta), Neustift (in red) and Monte Bondone (in blue) and a model parameterized grouping Monte Bondone and Neustift (M.Bondone&Neustift; in black). The black lines are 1:1 lines. Statistical significance is indicated as * ($p < 0.05$), ** ($p < 0.01$), and *** ($p < 0.001$).

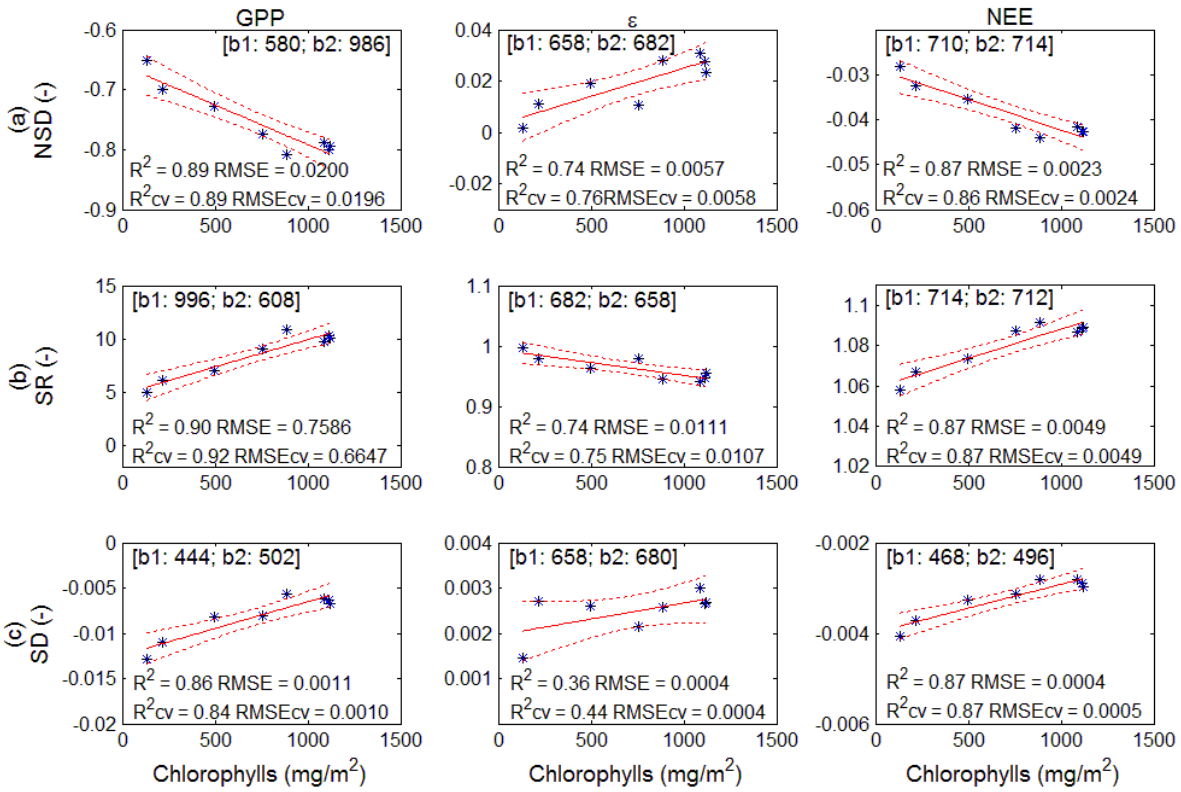

Figure S11. Correlation between selected (a) NSD-, (b) SR- and (c) SD-type indices and the total chlorophyll content for daily average ε and CO_2 fluxes (NEE and GPP) for Monte Bondone in 2013. R^2— coefficient of correlation for daily average of ε and CO_2 fluxes (NEE and GPP); RMSE—root mean square error; R^2cv— cross-validated coefficient of correlation; RMSEcv— cross-validated root mean square error. The solid red lines indicate the fitted models and the dotted red lines represent the 95% upper and lower confidence bounds. The selected bands to compute NSD-, SR- and SD-type indices are reported in brackets.

Tables

Table S1. Description of CO_2 flux measurements at the study sites.

Parameter	Amplero (IT-Amp)	Neustift (AT-Neu)	Monte Bondone (IT-MBo)
Sonic anemometer model	R3, Gill, Gill Instruments Ltd., Lymington, UK	R3, Gill, Instruments Ltd., Lymington, UK	R3, Gill Instruments Ltd., Lymington, UK
Infrared gas analyser model	Li-7500, Li-Cor Inc., Lincoln, Nebraska, USA	Li-7500, Li-Cor Inc., Lincoln, Nebraska, USA	Li-7500, Li-Cor Inc., Lincoln, Nebraska, USA
Data acquisition frequency (Hz)	20	20	20
Post-processing software	Developped by University of Viterbo (IT)	EdiRE (Version 1.4.3.1021, R. Clement, University of Edinburgh)	EdiRE (Version 1.4.3.1021, R. Clement, University of Edinburgh)
Outlier removal (method)	Wickers and Mahrt (1997)	-	-
CO_2/H_2O signal lag removal	Covariance maximization	Covariance maximization	Covariance maximization
Coordinate rotation (method)[1]	3D	3D	3D
Detrending of time series (method)	Linear detrending	-	-
Density corrections applied[2]	x	x	X
Sonic buoyancy to sensible heat flux conversion and cross-wind correction[3]	x	X	X

Low- and high-pass filtering corrected for (method)	Aubinet et al. (2000)	Moore (1986)	Aubinet et al. (2000)
Iterative calculation of fluxes[4]	-	X	-

[1] according to Wilczak et al. (2001); [2] according to Webb et al. (1980); [3] according to Schotanus et al. (1983); [4] according to Mauder et al. (2008)

Table S2. Description of the validation study sites and period.

Site characteristics	Längenfeld (AT-Lan)	Leutasch (AT-Leu)	Scharnitz (AT-Sch)
Latitude	47.0612	47.3780	47.3873
Longitude	10.9634	11.1627	11.2479
Elevation (m)	1180	1115	964
Mean annual temperature (˚C)	5.8	4.8	6.4
Mean annual precipitation (mm)	733	1309	1418
Vegetation type	*Phyteumo-Trisetion*	*Astrantio-Trisetetum*	*Arrenatherum montanum*
Study period[1]	163, 2006 (1)	227, 2006 (1)	184-284, 2006 (5)
Sonic anemometer model	R3, Gill Instruments Ltd., Lymington, UK	R3, Gill Instruments Ltd., Lymington, UK	R3, Gill Instruments Ltd., Lymington, UK
Infrared gas analyser model	Li-7500, Li-Cor Inc., Lincoln, Nebraska, USA	Li-7500, Li-Cor Inc., Lincoln, Nebraska, USA	Li-7500, Li-Cor Inc., Lincoln, Nebraska, USA
Data acquisition frequency (Hz)	20	20	20
Post-processing software	EdiRE (Version 1.4.3.1021, R. Clement, University of Edinburgh)	EdiRE (Version 1.4.3.1021, R. Clement, University of Edinburgh)	EdiRE (Version 1.4.3.1021, R. Clement, University of Edinburgh)
Outlier removal (method)	-	-	-
CO_2/H_2O signal lag removal	Covariance maximization	Covariance maximization	Covariance maximization
Coordinate rotation (method)[2]	3D	3D	3D
Detrending of time series (method)	-	-	-
Density corrections applied[3]	X	x	x
Sonic buoyancy to sensible heat flux conversion and cross-wind correction[4]	X	x	x
Low- and high-pass filtering corrected for (method)	Moore (1986)	Moore (1986)	Moore (1986)

[1] from-to DOY, year (number of hyperspectral measurement dates); [2] according to Wilczak et al. (2001); [3] according to Webb et al. (1980); [4] according to Schotanus et al. (1983); [5] according to Mauder et al. (2008).

Table S3. Results of statistic of linear regression models between VIs and daily average of ecophysiological parameters: ε, GPP and NEE. R^2—Coefficient of determination and RMSE—Root Mean Square Error. Bold letters indicate the best fitting model.

	ε								GPP								NEE							
	Amplero		Neustift		Monte Bondone		All		Amplero		Neustift		Monte Bondone		All		Amplero		Neustift		Monte Bondone		All	
	R^2	RMSE	R^2	RMSE	R^2	RMSE	R^2	RMSE	R^2	RMSE	R^2	RMSE	R^2	RMSE	R^2	RMSE	R^2	RMSE	R^2	RMSE	R^2	RMSE	R^2	RMSE
VI	-	$\frac{\mu mol_{CO2}}{\mu mol_{phot}}$	-	$\frac{\mu mol_{CO2}}{\mu mol_{phot}}$	-	$\frac{\mu mol_{CO2}}{\mu mol_{phot}}$	-	$\frac{\mu mol_{CO2}}{\mu mol_{phot}}$	-	$\frac{\mu mol_{CO2}}{m^2 s}$	-	$\frac{\mu mol_{CO2}}{m^2 s}$	-	$\frac{\mu mol_{CO2}}{m^2 s}$	-	$\frac{\mu mol_{CO2}}{m^2 s}$	-	$\frac{\mu mol_{CO2}}{m^2 s}$	-	$\frac{\mu mol_{CO2}}{m^2 s}$	-	$\frac{\mu mol_{CO2}}{m^2 s}$	-	
SR	**0.66**	0.01	0.33	0.04	0.33	0.04	0.13	0.04	**0.95**	0.73	0.25	2.63	0.71	2.30	0.26	4.92	0.91	0.90	0.25	1.96	0.69	1.60	0.24	3.40
GRI	0.39	0.01	**0.74**	0.02	0.43	0.04	**0.39**	0.04	0.81	1.39	0.16	2.64	**0.75**	2.12	0.07	5.51	0.83	1.23	0.16	2.06	0.67	1.65	0.09	3.72
WI	0.60	0.01	0.17	0.04	0.36	0.04	0.19	0.04	0.93	0.85	0.04	2.26	0.47	3.10	0.22	5.05	0.88	1.04	0.04	2.21	0.43	2.18	0.17	3.55
NDVI	0.51	0.01	0.31	0.04	0.48	0.04	0.29	0.04	0.88	1.09	**0.30**	2.60	0.73	2.19	0.35	4.60	0.88	1.02	**0.30**	1.89	0.77	1.39	0.34	3.16
SIPI	0.41	0.01	0.27	0.04	**0.55**	0.03	0.28	0.04	0.75	1.60	0.09	2.58	0.66	2.48	**0.48**	4.14	0.75	1.47	0.09	2.15	0.76	1.42	**0.48**	2.80
CI	0.54	0.01	0.70	0.02	0.38	0.04	0.25	0.04	0.94	0.76	0.13	2.65	0.73	2.22	0.14	5.29	**0.95**	0.65	0.13	2.11	0.77	1.38	0.16	3.57
PRI	0.49	0.01	0.14	0.04	0.32	0.04	0.36	0.04	0.44	2.37	0.06	2.44	0.17	3.86	0.12	5.36	0.44	2.21	0.06	2.19	0.21	2.56	0.07	3.76
EVI	0.53	0.01	0.42	0.03	0.51	0.03	0.28	0.04	0.86	1.17	0.12	2.63	0.60	2.69	0.32	4.71	0.87	1.05	0.12	2.11	0.66	1.67	0.27	3.33
NPQI	0.07	0.01	0.43	0.03	0.18	0.04	0.16	0.04	0.03	3.12	0.00	2.64	0.12	3.98	0.22	5.04	0.12	2.78	0.00	2.25	0.12	2.69	0.17	3.55
NPCI	0.45	0.01	0.13	0.04	0.00	0.05	0.01	0.04	0.60	2.01	0.01	2.47	0.18	3.83	0.38	4.51	0.67	1.71	0.01	2.25	0.26	2.47	0.36	3.11
SRPI	0.47	0.01	0.11	0.04	0.00	0.05	0.01	0.04	0.55	2.13	0.01	2.47	0.19	3.80	0.34	4.64	0.62	1.82	0.01	2.25	0.27	2.46	0.32	3.21
RedEdgeNDVI	0.52	0.01	0.72	0.02	0.42	0.04	0.29	0.04	0.93	0.82	0.12	2.65	0.73	2.20	0.18	5.20	0.95	0.67	0.12	2.11	**0.78**	1.35	0.19	3.50

Table S4. Results of validation of linear regression models between VIs ((a) NSD-type; (b) SR-type; (c) SD-type) and ecophysiological parameters: α, ε (midday average), GPP_{max} and midday average CO_2 fluxes (NEE and GPP). Validation was performed by applying the three different models for Amplero, Neustift, Monte Bondone and a model parameterized grouping Neustift and Monte Bondone (M.Bondone&Neustift). slope—slope of linear model; y-int—intercept of linear model, and RMSE—Root Mean Square Error.

Model	α			GPPmax			GPP			ε			NEE		
	slope	y-int	RMSE	slope	y-int	RMSE	slope	y-int	RMSE	slope	y-int	RMSE	slope	y-int	RMSE
	-	$\frac{\mu mol_{CO2}}{\mu mol_{phot}}$	$\frac{\mu mol_{CO2}}{\mu mol_{phot}}$	-	$\frac{\mu mol_{CO2}}{m^2 s}$	$\frac{\mu mol_{CO2}}{m^2 s}$	-	$\frac{\mu mol_{CO2}}{m^2 s}$	$\frac{\mu mol_{CO2}}{m^2 s}$	-	$\frac{\mu mol_{CO2}}{\mu mol_{phot}}$	$\frac{\mu mol_{CO2}}{\mu mol_{phot}}$	-	$\frac{\mu mol_{CO2}}{m^2 s}$	$\frac{\mu mol_{CO2}}{m^2 s}$
(a) NSD-type															
Amplero	0.22	0.01	0.03	0.24	5.69	9.37	0.67	-5.30	11.51	-1.99	0.05	0.02	0.06	-0.89	11.78
Neustift	-2.63	0.16	0.17	0.66	10.13	4.80	0.75	7.59	3.64	-7.37	0.15	0.06	0.28	-9.74	9.00
Monte Bondone	-0.15	0.05	0.02	0.51	12.69	5.19	0.88	6.20	4.81	-1.88	0.10	0.06	0.54	-11.78	8.17
M.Bondone&Neustift	2.94	-0.05	0.04	0.67	10.88	6.59	0.63	7.40	4.78	-4.25	0.10	0.08	0.24	-9.02	9.00
(b) SR-type															
Amplero	0.22	0.01	0.03	0.24	5.71	9.37	0.67	-5.25	11.52	-1.96	0.05	0.02	0.06	-0.90	11.77
Neustift	-2.59	0.16	0.17	0.67	9.99	4.77	0.74	7.85	3.69	-7.37	0.15	0.06	0.27	-9.79	8.99
Monte Bondone	-0.14	0.05	0.02	0.56	11.43	5.23	0.99	4.60	5.26	-1.88	0.10	0.06	0.46	-12.30	8.36
M.Bondone&Neustift	0.93	0.05	0.05	0.67	10.81	6.58	0.67	6.75	4.81	-3.61	0.12	0.05	0.25	-8.97	9.01
(c) SD-type															
Amplero	0.11	0.01	0.03	-0.18	12.80	10.74	0.65	-5.09	11.73	2.52	-0.03	0.02	-0.08	-13.04	9.48
Neustift	2.71	0.04	0.15	-0.48	28.93	9.75	0.53	12.63	5.57	0.30	0.01	0.07	-0.33	-21.85	13.17
Monte Bondone	0.07	0.04	0.02	0.77	8.39	5.39	0.62	12.75	7.23	-0.89	0.09	0.06	0.40	-14.56	9.85
M.Bondone&Neustift	-0.05	0.06	0.03	0.68	11.36	6.39	0.67	10.70	5.59	-0.86	0.09	0.06	0.39	-13.66	8.92

Table S5. Results of validation of linear regression models between VIs ((a) NSD-type; (b) SR-type; (c) SD-type) and ecophysiological parameters: for the daily averaged GPP, ε and NEE. Validation was performed by applying the three different models for Amplero, Neustift, Monte Bondone and a model parameterized grouping Neustift and Monte Bondone (M.Bondone&Neustift). slope—slope of linear model; y-int—intercept of linear model, and RMSE—Root Mean Square Error.

Model	GPP			ε			NEE		
	slope	y-int	RMSE	slope	y-int	RMSE	slope	y-int	RMSE
	-	$\frac{\mu mol_{CO2}}{m^2 s}$	$\frac{\mu mol_{CO2}}{m^2 s}$	-	$\frac{\mu mol_{CO2}}{\mu mol_{phot}}$	$\frac{\mu mol_{CO2}}{\mu mol_{phot}}$	-	$\frac{\mu mol_{CO2}}{m^2 s}$	$\frac{\mu mol_{CO2}}{m^2 s}$
(a) NSD-type									
Amplero	0.11	4.80	13.04	-0.18	0.02	0.01	0.26	-0.74	9.39
Neustift	0.25	13.90	5.07	-2.59	0.05	0.08	-0.04	-11.91	9.06
Monte Bondone	0.32	9.00	5.38	-1.44	0.11	0.07	0.24	-7.12	6.27
M.Bondone&Neustift	0.21	12.18	5.70	-3.90	0.10	0.08	0.13	-8.59	6.88
(b) SR-type									
Amplero	0.11	4.80	13.04	-0.18	0.02	0.01	0.26	-0.76	9.40
Neustift	-0.34	19.60	9.94	-2.76	0.05	0.07	-0.05	-11.79	9.09
Monte Bondone	0.36	7.89	5.65	-1.45	0.11	0.07	0.24	-7.13	6.27
M.Bondone&Neustift	0.22	12.12	5.67	-3.92	0.10	0.08	0.12	-8.78	6.98
(c) SD-type									
Amplero	0.35	-0.61	13.13	0.88	0.00	0.01	-0.02	-5.40	9.79
Neustift	0.24	14.09	5.06	0.33	0.02	0.07	0.07	-9.68	7.38
Monte Bondone	0.50	6.00	5.67	-1.47	0.10	0.05	0.32	-6.51	5.78
M.Bondone&Neustift	0.26	12.69	4.51	-0.70	0.04	0.06	0.27	-9.25	6.37

Table S6. Results of the correlation (R^2—Coefficient of determination) between the best NDS, SR and SD-type indices selected for the daily averaged GPP, ε and NEE and dry phytomass, nitrogen and water content for Amplero, Neustift, Monte Bondone and all sites pooled. Statistical significance is indicated as * ($p < 0.05$), ** ($p < 0.01$), and *** ($p < 0.001$).

Index	Site	Parameter	GPP R^2 (-)	ε R^2 (-)	NEE R^2 (-)
NSD-type	Amplero	Dry phytomass (g m^{-2})	0.67**	0.79**	0.69**
	Amplero	Nitrogen content (%)	0.38	0.29	0.31
	Amplero	Water content (%)	0.66**	0.28	0.72**
	Neustift	Dry phytomass (g m^{-2})	0.02	0.29	0.06
	Neustift	Nitrogen content (%)	0.07	0.83**	0.02
	Neustift	Water content (%)	0.04	0.64*	0.00
	Monte Bondone	Dry phytomass (g m^{-2})	0.56***	0.48***	0.27*
	Monte Bondone	Nitrogen content (%)	0.50***	0.44***	0.25*
	Monte Bondone	Water content (%)	0.45	0.37	0.18
	All	Dry phytomass (g m^{-2})	0.02	0.04	0.00
	All	Nitrogen content (%)	0.04	0.46***	0.10*
	All	Water content (%)	0.01	0.13*	0.01
SR-type	Amplero	Dry phytomass (g m^{-2})	0.67**	0.81*	0.69**
	Amplero	Nitrogen content (%)	0.37	0.30	0.31
	Amplero	Water content (%)	0.66**	0.28	0.72**
	Neustift	Dry phytomass (g m^{-2})	0.02	0.29	0.06
	Neustift	Nitrogen content (%)	0.00	0.85**	0.03

	Neustift	Water content (%)	0.15	0.64*	0.00
	Monte Bondone	Dry phytomass (g m^{-2})	0.55***	0.49***	0.27*
	Monte Bondone	Nitrogen content (%)	0.49***	0.45***	0.24*
	Monte Bondone	Water content (%)	0.45***	0.38	0.18*
	All	Dry phytomass (g m^{-2})	0.01	0.05	0.00
	All	Nitrogen content (%)	0.03	0.45***	0.10
	All	Water content (%)	0.01	0.14*	0.01
SD-type	Amplero	Dry phytomass (g m^{-2})	0.66**	0.79**	0.71**
	Amplero	Nitrogen content (%)	0.24	0.26	0.31*
	Amplero	Water content (%)	0.58*	0.35	0.71**
	Neustift	Dry phytomass (g m^{-2})	0.02	0.20	0.01
	Neustift	Nitrogen content (%)	0.11	0.81**	0.45
	Neustift	Water content (%)	0.06	0.64*	0.09
	Monte Bondone	Dry phytomass (g m^{-2})	0.32**	0.52***	0.22*
	Monte Bondone	Nitrogen content (%)	0.31**	0.45***	0.30**
	Monte Bondone	Water content (%)	0.32**	0.40***	0.23
	All	Dry phytomass (g m^{-2})	0.08	0.19**	0.03
	All	Nitrogen content (%)	0.02	0.31***	0.00
	All	Water content (%)	0.02	0.03	0.00